Long-term thermal sensitivity of Earth's tropical forests

Martin J P Sullivan, Simon Lewis, Kofi Affum-Baffoe, Carolina Castilho,
Flávia Costa, Aida Cuni Sanchez, Corneille Ewango, Wannes Hubau, Beatriz
Marimon, Abel Monteagudo-Mendoza, et al.

Long-term thermal sensitivity of Earth's tropical forests

Martin J. P. Sullivan[1,2], Simon L. Lewis[1,3], Kofi Affum-Baffoe[4], Carolina Castilho[5], Flávia Costa[6], Aida Cuni Sanchez[7,8], Corneille E. N. Ewango[9,10,11], Wannes Hubau[1,12,13], Beatriz Marimon[14], Abel Monteagudo-Mendoza[15], Lan Qie[16], Bonaventure Sonké[17], Rodolfo Vasquez Martinez[15], Timothy R Baker[1], Roel J. W. Brienen[1], Ted R. Feldpausch[18], David Galbraith[1], Manuel Gloor[1], Yadvinder Malhi[19], Shin-Ichiro Aiba[20], Miguel N. Alexiades[21], Everton C. Almeida[22], Edmar Almeida de Oliveira[23], Esteban Álvarez Dávila[24], Patricia Alvarez Loayza[25], Ana Andrade[26], Simone Aparecida Vieira[27], Luiz Aragão[28], Alejandro Araujo-Murakami[29], Eric J.M.M. Arets[30], Luzmila Arroyo[31], Peter Ashton[32], Gerardo Aymard C.[33], Fabrício B. Baccaro[34], Lindsay F. Banin[35], Christopher Baraloto[36], Plínio Barbosa Camargo[37], Jos Barlow[38], Jorcely Barroso[39], Jean-François Bastin[40], Sarah A. Batterman[1,41,42,43], Hans Beeckman[12], Serge K. Begne[17,44], Amy C. Bennett[44], Erika Berenguer[19,38], Nicholas Berry[45], Lilian Blanc[46], Pascal Boeckx[47], Jan Bogaert[48], Damien Bonal[49], Frans Bongers[50], Matt Bradford[51], Francis Q. Brearley[2], Terry Brncic[52], Foster Brown[53], Benoit Burban[54], José Luís Camargo[26], Wendeson Castro[55], Carlos Céron[56], Sabina Cerruto Ribeiro[57], Victor Chama Moscoso[15], Jérôme Chave[58], Eric Chezeaux[59], Connie J. Clark[25], Fernanda Coelho[1], Murray Collins[61], James A. Comiskey[62,63], Fernando Cornejo Valverde[64], Massiel Corrales Medina[65], Lola da Costa[66], Martin Dančák[67], Greta C. Dargie[1], Stuart Davies[68], Nallaret Davila Cardozo[69], Thales de Haulleville[12,48], Marcelo Brilhante de Medeiros[70], Jhon del Aguila Pasquel[71], Géraldine Derroire[72], Anthony Di Fiore[73], Jean-Louis Doucet[74], Aurélie Dourdain[72], Vincent Droissant[75], Luisa Fernanda Duque[76], Romeo Ekoungoulou[77], Fernando Elias[78], Terry Erwin[79], Adriane Esquivel-Muelbert[80], Sophie Fauset[81], Joice Ferreira[82], Gerardo Flores Llampazo[83], Ernest Foli[84], Andrew Ford[51], Martin Gilpin[1], Jefferson S. Hall[85], Keith C. Hamer[86], Alan C. Hamilton[87], David J. Harris[88], Terese B. Hart[89,90], Radim Hédl[91,92], Bruno Herault[72], Rafael Herrera[93], Niro Higuchi[6], Annette Hladik[94], Eurídice Honorio Coronado[71], Isau Huamantupa-Chuquimaco[95], Walter Huaraca Huasco[95], Kathryn J. Jeffery[96], Eliana Jimenez-Rojas[97], Michelle Kalamandeen[1], Marie-Noel Kamdem[11,13,17,98], Elizabeth Kearsley[99], Ricardo Keichi Umetsu[100], Lip Khoon Kho Khoon[101], Timothy Killeen[102], Kanehiro Kitayama[103], Bente Klitgaard[104], Nicolas Labrière[58], William Laurance[105], Susan Laurance[105], Miguel E. Leal[106], Aurora Levesley[1], Adriano J. N. Lima[6], Janvier Lisingo[11], Aline P. Lopes[107,108], Gabriela Lopez-Gonzalez[1], Tom Lovejoy[109], Jon Lovett[1], Richard Lowe[110], William E. Magnusson[111], Jagoba Malumbres-Olarte[112,113], Ângelo Gilberto Manzatto[114], Ben Hur Marimon Junior[115], Andrew R. Marshall[8,116,117], Toby Marthews[118], Simone Matias de Almeida Reis[14,19], Colin Maycock[119], Karina Melgaço[1], Casimiro Mendoza[120], Faizah Metali[121], Vianet Mihindou[122,123], William Milliken[104], Edward Mitchard[124], Paulo S. Morandi[14], Hannah L. Mossman[2], Laszlo Nagy[125], Henrique Nascimento[6], David Neill[126], Reuben Nilus[127], Percy Núñez Vargas[95], Walter Palacios[128], Nadir Pallqui Camacho[1,95], Julie Peacock[1], Colin Pendry[129], Maria Cristina Peñuela Mora[130], Georgia C. Pickavance[1], John Pipoly[131], Nigel Pitman[132], Maureen Playfair[133], Lourens Poorter[134], John R. Poulsen[25], Axel D. Poulsen[135], Richard Preziosi[2], Adriana Prieto[136], Richard Primack[137], Hirma Ramírez-Angulo[138], Jan Reitsma[139], Maxime Réjou-Méchain[75], Zorayda Restrepo Correa[140], Thaiane Rodrigues de Sousa[6], Lily Rodriguez Bayona[141], Anand Roopsind[142], Agustín Rudas[136], Ervan Rutishauser[42,143], Kamariah Abu Salim[121], Rafael P. Salomão[144,145], Juliana Schietti[6], Douglas Sheil[146], Richarlly C. Silva[57,147], Javier Silva Espejo[148], Camila Silva Valeria[38], Marcos Silveira[57], Murielle Simo-Droissart[17], Marcelo Fragomeni Simon[70], James Singh[149], Yahn Carlos Soto Shareva[15], Clement Stahl[54], Juliana Stropp[150], Rahayu Sukri[121], Terry Sunderland[151,152], Martin Svátek[153], Michael D. Swaine[154], Varun Swamy[155], Hermann Taedoumg[17], Joey Talbot[1], James Taplin[156], David Taylor[157], Hans ter Steege[158,159], John Terborgh[25], Raquel Thomas[142], Sean C. Thomas[160], Armando Torres-Lezama[161], Peter Umunay[162,163], Luis Valenzuela Gamarra[15], Geertje van der Heijden[164], Peter van der Hout[165], Peter van der Meer[166], Mark van Nieuwstadt[167], Hans Verbeeck[99], Ronald Vernimmen[168], Alberto Vicentini[6], Ima Célia Guimarães Vieira[145], Emilio Vilanova Torre[169], Jason Vleminckx[36], Vincent Vos[171], Ophelia Wang[172], Lee J. T. White[123,173,174], Simon Willcock[175], John T. Woods[176], Verginia Wortel[177], Kenneth Young[178], Roderick Zagt[179], Lise Zemagho[17], Pieter A. Zuidema[50], Joeri A. Zwerts[177,180], Oliver L. Phillips[1]

1

Affiliations:

1   School of Geography, University of Leeds, Leeds, UK

2   Department of Natural Sciences, Manchester Metropolitan University, Manchester, UK

3   Department of Geography, University College London, London, UK

4   Mensuration Unit, Forestry Commission of Ghana, Kumasi, Ghana

5   Embrapa Roraima, Brazilian Agricultural Research Corporation (EMBRAPA), Brasília, Brazil

6   Instituto Nacional de Pesquisas da Amazônia (INPA), Manaus, Brazil

7   Department of Ecosystem Science and Sustainability, Colorado State University, USA

8   Department of Environment and Geography, University of York, York, UK

9   DR Congo Programme, Wildlife Conservation Society, Kisangani, Democratic Republic of Congo

10   Centre de Formation et de Recherche en Conservation Forestiere (CEFRECOF), Epulu, Democratic Republic of Congo

11   Faculté de Gestion de Ressources Naturelles Renouvelables, Université de Kisangani, Kisangani, Democratic Republic of Congo

12   Service of Wood Biology, Royal Museum for Central Africa, Tervuren, Belgium

13   Department of Environment, Laboratory of Wood Technology (Woodlab), Ghent University, Ghent, Belgium

14   Faculdade de Ciências Agrárias, Biológicas e Sociais Aplicadas, Universidade do Estado de Mato Grosso, Nova Xavantina-MT, Brazil

15   Jardín Botánico de Missouri, Oxapampa, Peru

16   School of Life Sciences, University of Lincoln, Lincoln, UK

17   Plant Systematics and Ecology Laboratory, Higher Teachers' Training College, University of Yaoundé I, Yaoundé, Cameroon

18   Geography, College of Life and Environmental Sciences, University of Exeter, Exeter, UK

19   Environmental Change Institute, School of Geography and the Environment, University of Oxford, Oxford, UK

20   Graduate School of Science and Engineering, Kagoshima University, Japan

21   School of Anthropology and Conservation, University of Kent, Canterbury, UK

22   Instituto de Biodiversidade e Florestas, Universidade Federal do Oeste do Pará, Santarém - PA, Brazil

23   Universidade do Estado de Mato Grosso, Cáceres - MT, Brazil

24   Escuela de Ciencias Agrícolas, Pecuarias y del Medio Ambiente, National Open University and Distance, Colombia

25   Center for Tropical Conservation, Nicholas School of the Environment, Duke University, Durham, NC, USA

26   Projeto Dinâmica Biológica de Fragmentos Florestais, Instituto Nacional de Pesquisas da Amazônia, Manaus, Brazil

27   Universidade Estadual de Campinas, Campinas - SP, Brazil

28   National Institute for Space Research (INPE), São José dos Campos-SP, Brazil

29   Museo de Historia Natural Noel Kempff Mercado, Universidad Autónoma Gabriel René Moreno, Santa Cruz, Bolivia

30   Wageningen Environmental Research, Wageningen, The Netherlands

31   Dirección de la Carrera de Biología, Universidad Autónoma Gabriel René Moreno, Santa Cruz, Bolivia

32   Department of Organismic and Evolutionary Biology, Harvard University, Cambridge, MA, USA

33   Programa de Ciencias del Agro y el Mar, Herbario Universitario, Barinas, Venezuela

34   Departamento de Biologia, Universidade Federal do Amazonas, Manaus, Brazil

[35]   Centre of Ecology and Hydrology, Penicuik, UK

[36]   International Center for Tropical Botany, Department of Biological Sciences, Florida International University, Florida, FL, USA

[37]   Centro de Energia Nuclear na Agricultura, Universidade de São Paulo, São Paulo, SP, Brazil

[38]   Lancaster Environment Centre, Lancaster University, Lancaster, UK

[39]   Centro Multidisciplinar, Universidade Federal do Acre, Cruzeiro do Sul - AC, Brazil

[40]   Institure of Integrative Biology, ETH Zurich, Zurich, Switzerland

[41]   Priestley International Centre for Climate, University of Leeds, Leeds, UK

[42]   Smithsonian Tropical Research Institute, Panama, Panama

[43]   Cary Institute of Ecosystem Studies, Millbrook, NY, USA

[44]   School of Geography, School of Geography, Leeds, UK

[45]   The Landscapes and Livelihoods Group, Edinburgh, UK

[46]   UR Forest& Societies, CIRAD, Montpellier, France

[47]   Isotope Bioscience Laboratory-ISOFYS, Ghent University, Gent, Belgium

[48]   Gembloux Agro-Bio Tech, University of Liège, Liège, Belgium

[49]   UMR Silva, INRA, Nancy, France

[50]   Department of Forest Ecology and Forest Management Group, Wageningen University, Wageningen, The Netherlands

[51]   CSIRO, Canberra, Australia

[52]   Congo Programme, Wildlife Conservation Society, Brazzavile, Republic of Congo

[53]   Woods Hole Research Center, Falmouth, MA, USA

[54]   Ecologie des Forêts de Guyane (ECOFOG), INRA, Kourou, French Guiana

[55]   Programa de Pós-Graduação Ecologia e Manejo de Recursos Naturais, Universidade Federal do Acre, Rio Branco - AC, Brazil

[56]   Herbario Alfredo Paredes, Universidad Central del Ecuador, Quito, Ecuador

[57]   Centro de Ciências Biológicas e da Natureza, Universidade Federal do Acre, Rio Branco - AC, Brazil

[58]   Laboratoire Évolution et Diversité Biologique - UMR 5174 (CNRS/IRD/UPS), CNRS, Toulouse, France

[59]   Rougier-Gabon, Libreville, Gabon

[60]   Nicholas School of the Environment, Duke University, Durham, NC, USA

[61]   Grantham Research Institute on Climate Change and the Environment, London, UK

[62]   Inventory & Monitoring Program, National Park Service, Fredericksburg, VA, USA

[63]   Smithsonian Institution, Washington, DC, USA

[64]   Proyecto Castaña, Made de Dios, Peru

[65]   Universidad Nacional de San Agustín de Arequipa, Arequipa, Peru

[66]   Instituto de Geociências, Faculdade de Meteorologia, Universidade Federal do Para, Belém - PA, Brazil

[67]   Faculty of Science, Department of Ecology and Environmental Sciences, Palacký University Olomouc, Olomouc, Czech Republic

[68]   Center for Tropical Forest Science, Smithsonian Tropical Research Institute, Panama, Panama

[69]   Facultad de Ciencias Biológicas, Universidad Nacional de la Amazonía Peruana, Iquitos, Peru

[70]   Embrapa Genetic Resources & Biotechnology, Brazilian Agricultural Research Corporation (EMBRAPA), Brasília, Brazil

[71]   Instituto de Investigaciones de la Amazonía Peruana, Iquitos, Peru

[72]   Ecologie des Forêts de Guyane (ECOFOG), CIRAD, Kourou, French Guiana

73 Department of Anthropology, The University of Texas at Austin, Austin, TX, USA

74 Forest Resources Management, Gembloux Agro-Bio Tech, University of Liège, Liège, Belgium

75 AMAP Lab, IRD, CIRAD, CNRS, INRA, Univ Montpellier, Montpellier, France

76 Socioecosistemas y Cambio Climatico, Fundacion con Vida, Medellín, Colombia

77 School of Forestry, Beijing Forestry University, Beijing, China

78 Institute of Biological Sciences, Universidade Federal do Pará, Belém - PA, Brazil

79 National Museum of Natural History, Smithsonian Institute, Washington, DC, USA

80 School of Geography, Earth and Environmental Sciences, University of Birmingham, Birmingham, UK

81 School of Geography, Earth and Environmental Sciences, University of Plymouth, Plymouth, UK

82 Embrapa Amazônia Oriental, Brazilian Agricultural Research Corporation (EMBRAPA), Brasília, Brazil

83 Universidad Nacional Jorge Basadre de Grohmann (UNJBG), Tacna, Peru

84 Forestry Research Institute of Ghana (FORIG), Kumasi, Ghana

85 Smithsonian Institution Forest Global Earth Observatory (ForestGEO), Smithsonian Tropical Research Institute, Washington, DC, USA

86 School of Biology, University of Leeds, Leeds, UK

87 128 Busbridge Lane, Godalming, Surrey, UK

88 Royal Botanic Garden Edinburgh, Edinburgh, UK

89 Lukuru Wildlife Research Foundation, Kinshasa, Democratic Republic of Congo

90 Division of Vertebrate Zoology, Yale Peabody Museum of Natural History, New Haven, CT, USA

91 Institute of Botany, Czech Academy of Sciences, Brno, Czech Republic

92 Department of Botany, Palacký University in Olomouc, Olomouc, Czech Republic

93 Instituto Venezolano de Investigaciones Científicas (IVIC), Caracas, Venezuela

94 Département Hommes, natures, sociétés, Muséum National d'Histoire Naturel, Paris, France

95 Universidad Nacional de San Antonio Abad del Cusco, Cusco, Peru

96 Biological and Environmental Sciences, University of Stirling, Stirling, UK

97 Instituto IMANI, Universidad Nacional de Colombia, Leticia, Colombia

98 Faculty of Science, Department of Botany and Plant Physiology, University of Buea, Buea, Cameroon

99 Department of Environment, Computational & Applied Vegetation Ecology (Cavelab), Ghent University, Ghent, Belgium

100 PELD, Universidade do Estado de Mato Grosso, Nova Xavantina-MT, Brazil

101 Tropical Peat Research Institute, Malaysian Palm Oil Board, Kuala Lumpur, Malaysia

102 Agteca, Santa Cruz, Bolivia

103 Graduate School of Agriculture, Kyoto University, Japan

104 Royal Botanic Gardens Kew, Richmond, London, UK

105 Centre for Tropical Environmental and Sustainability Science (TESS) and College of Marine and Environmental Sciences, James Cook University, Australia

106 Uganda Programme, Wildlife Conservation Society, Kampala, Uganda

107 Remote Sensing Division, National Institute for Space Research (INPE), São José dos Campos-SP, Brazil

108 Department of Ecology, University of Brasília, Brasília, Brazil

109 Environmental Science and Policy, George Mason University, Fairfax, VA, USA

110 Botany Department, University of Ibadan, Ibadan, Nigeria

[111] Coordenação da Biodiversidade, Instituto Nacional de Pesquisas da Amazônia (INPA), Mauaus, Brazil

[112] cE3c – Centre for Ecology, Evolution and Environmental Changes / Azorean Biodiversity Group, Universidade dos Açores, Angra do Heroísmo, Azores, Portugal

[113] LIBRe – Laboratory for Integrative Biodiversity Research, Finnish Museum of Natural History, University of Helsinki, Helsinki, Finland

[114] Laboratório de Biogeoquímica Ambiental Wolfgang C. Pfeiffer, Universidade Federal de Rondônia, Porto Velho - RO, Brazil

[115] Faculdade de Ciências Agrárias, Biológicas e Sociais Aplicadas, Universidad do Estado de Mato Grosso, Nova Xavantina-MT, Brazil

[116] Tropical Forests and People Research Centre, University of the Sunshine Coast, Australia

[117] Flamingo Land Ltd., North Yorkshire, UK

[118] Centre for Ecology and Hydrology, Wallingford, UK

[119] School of International Tropical Forestry, Universiti Malaysia Sabah, Kota Kinabalu, Malaysia

[120] Escuela de Ciencias Forestales, Unidad Académica del Trópico, Universidad Mayor de San Simón, Sacta, Bolivia

[121] Faculty of Science, Universiti Brunei Darussalam, Brunei

[122] Agence Nationale des Parcs Nationaux, Libreville, Gabon

[123] Ministère de la Forêt, de la Mer, de l'Environnement, Chargé du Plan Climat, Libreville, Gabon

[124] University of Edinburgh, Edinburgh, UK

[125] Biologia Vegetal, Universide Estadual de Campinas, Campinas - SP, Brazil

[126] Facultad de Ingeniería Ambiental, Universidad Estatal Amazónica, Puyo, Pastaza, Ecuador

[127] Forest Research Centre, Sabah Forestry Department, Sepilok, Malaysia

[128] Carrera de Ingeniería Forestal, Universidad Tecnica del Norte, Ibarra, Ecuador

[129] Royal Botanical Garden Edinburgh, Edinburgh, UK

[130] Universidad Regional Amazónica IKIAM, Tena, Ecuador

[131] Public Communications and Outreach Group, Parks and Recreation Division, Oakland Park, FL, USA

[132] Keller Science Action Center, Field Museum, Chicago, IL, USA

[133] Centre for Agricultural Research in Suriname (CELOS), Paramaribo, Suriname

[134] Department of Forest Ecology and Forest Management Group, Wageningen University and Research, Wageningen, The Netherlands

[135] University of Oslo, Oslo, Norway

[136] Instituto de Ciencias Naturales, Universidad Nacional de Colombia, Leticia, Colombia

[137] Department of Biology, Boston University, Boston, USA

[138] Institute of Research for Forestry Development (INDEFOR), Universidad de los Andes, Mérida, Venezuela

[139] Bureau Waardenburg, Culemborg, The Netherlands

[140] Socioecosistemas y Cambio Climatico, Fundacion Con Vida, Medellín, Colombia

[141] Centro de Conservacion, Investigacion y Manejo de Areas Naturales, CIMA Cordillera Azul, Lima, Peru

[142] Iwokrama International Centre for Rainforest Conservation and Development, Georgetown, Guyana

[143] Carboforexpert, Geneva, Switzerland

[144] Universidade Federal Rural da Amazônia/CAPES, Belém - PA, Brazil

[145] Museu Paraense Emílio Goeldi, Belém - PA, Brazil

[146] Faculty of Environmental Sciences and Natural Resource Management, Norwegian University of Life Sciences, Ås, Norway

[147] Instituto Federal do Acre, Rio Branco - AC, Brazil

[148]   Universidad de San Antonio Abad del Cusco, Cusco, Peru

[149]   Guyana Forestry Commission, Georgetown, Guyana

[150]   Federal University of Alagoas, Maceió, Brazil

[151]   Sustainable Landscapes and Food Systems, Center for International Forestry Research, Bogor, Indonesia

[152]   Faculty of Forestry, University of British Columbia, Vancouver, Canada

[153]   Department of Forest Botany, Dendrology and Geobiocoenology, Mendel University in Brno, Brno, Czech Republic

[154]   Department of Plant & Soil Science, School of Biological Sciences, University of Aberdeen, Aberdeen, UK

[155]   Institute for Conservation Research, San Diego Zoo, San Diego, USA

[156]   UK Research & Innovation, Innovate UK, London

[157]   Department of Geography, National University of Singapore, Singapore, Singapore

[158]   Naturalis Biodiversity Center, Leiden, The Netherlands

[159]   Systems Ecology, VU University, Amsterdam, The Netherlands

[160]   Faculty of Forestry, University of Toronto, Toronto, Canada

[161]   Universidad de los Andes, Merida, Colombia

[162]   Wildlife Conservation Society, New York, NY, USA

[163]   Yale School of Forestry & Environmental Studies, Yale University, New Haven, CT, USA

[164]   School of Geography, University of Notingham, Nottingham, UK

[165]   Van der Hoult Forestry Consulting, Rotterdam, The Netherlands

[166]   Van Hall Larenstein University of Applied Sciences, Velp, The Netherlands

[167]   Utrecht University, Utrecht, The Netherlands

[168]   Deltares, Delft, The Netherlands

[169]   School of Environmental and Forest Sciences, University of Washington, Seattle, OR, USA

[170]   Department of Biological Sciences, Florida International University, Florida, FL, USA

[171]   Centro de Investigación y Promoción del Campesinado, La Paz, Bolivia

[172]   School of Earth Sciences and Environmental Sustainability, Northern Arizona University, Flagstaff, AZ, USA

[173]   Institut de Recherche en Ecologie Tropicale, Libreville, Gabon

[174]   School of Natural Sciences, University of Stirling, Stirling, UK

[175]   School of Natural Sciences, University of Bangor, Bangor, UK

[176]   University of Liberia, Monrovia, Liberia

[177]   Forest Management, Centre for Agricultural Research in Suriname (CELOS), Paramaribo, Suriname

[178]   Department of Geography and The Environment, University of Texas at Austin, Austin, TX, USA

[179]   Tropenbos International, Wageningen, The Netherlands

[180]   Biology, Utrecht University, Utrecht, The Netherlands

1 **Abstract**

2 The sensitivity of tropical forest carbon to climate is a key uncertainty in predicting global climate

3 change. While short-term drying and warming are known to impact forests it is unknown if such effects

4 translate into long-term responses. Here we analyse 590 permanent plots measured across the tropics to

5 derive the equilibrium climate controls on forest carbon. Maximum temperature is the most important

6 predictor of aboveground biomass (-9.1 Mg C ha^{-1} °C^{-1}), primarily by reducing woody productivity, and

7 with a greater rate of decline in the hottest forests. Our results nevertheless reveal greater thermal

8 resilience than observations of short-term variation imply. Realising the long-term climate adaptation

9 potential of tropical forests will require both protecting them and stabilising the Earth's climate.

10

11

12 **One sentence summary.** Biome-wide variation in tropical forest carbon stocks and dynamics shows

13 long-term thermal resilience.

7

14 <u>Main text</u>

15 The response of tropical terrestrial carbon to environmental change is a critical component of global

16 climate models (*1*). Land-atmosphere feedbacks depend on the balance of positive biomass growth

17 stimulation by CO_2 fertilisation (i.e. β) and negative responses to warmer temperatures and any

18 change in precipitation (i.e. γ). Yet the climate response is so poorly constrained that it remains one of

19 the largest uncertainties in Earth system models (*2, 3*), with the temperature sensitivity of tropical land

20 carbon stocks alone differing by > 100 Pg C $°C^{-1}$ among models (*2*). Such uncertainty impedes our

21 understanding of the global carbon cycle, limiting our ability to simulate the future of the Earth

22 system under different long-term climate mitigation strategies. A critical long-term control on tropical

23 land-atmosphere feedbacks is the sensitivity to climate (γ) of tropical forests, where c. 40 % of the

24 world's vegetation carbon resides (*4*).

25 The sensitivity of tropical biomass carbon stocks, their rate of production and their persistence to

26 environmental change can all be estimated by relating their short-term and inter-annual responses to

27 variation in climate (*5-7*). These sensitivities are then used to constrain longer-term projections of

28 climate responses (*2*). Such approaches typically find that higher minimum temperatures are strongly

29 associated with slower tree growth and reduced forest carbon stocks, likely due to increased

30 respiration at higher temperatures (*7-9*). Tropical forest carbon is also sensitive to precipitation (*10*),

31 with, for example, elevated tree mortality occurring during drought events (*11*).

32 Yet, the sensitivity of ecosystems to inter-annual fluctuations may be an unreliable guide to their

33 longer-term responses to climate change. Such responses will also be influenced by physiological

34 acclimation (*12*), changes in demographic rates (*13*), and shifts in species composition (*14*). For

35 example, both respiration and photosynthesis can acclimate under sustained temperature increases

36 (*15-17*), and tropical trees exhibit physiological plasticity (*18*) and shifts in species composition (*14*)

37 under sustained drought. These processes could mean that tropical forests are less sensitive to climate

38 than estimates derived from inter-annual variability imply. An alternative, complimentary approach to

39 assessing sensitivity to climate is to measure and analyse spatial variation in tropical ecosystems

40 across climate gradients as a space-for-time substitution. Such biome-wide spatial variation in forest

8

41 carbon stocks, fluxes and persistence offers a unique and largely unexplored window into the potential

42 equilibrium sensitivity of tropical forest vegetation to warming, as it captures real-world vegetation

43 responses that allow for physiological and ecological adaptation (*12*).

44 To assess the long-term climate controls on tropical forest growth and carbon stocks, here we have

45 assembled, measured, and analysed a pan-tropical network of 590 permanent, long-term inventory

46 plots (Fig. 1, see Figs. S1-2 for ability to capture biome climate space). Our analysis combines

47 standardised measurements from across South American, African, Asian and Australian tropical

48 lowland forests (273, 239, 61 and 17 plots respectively). For every plot we calculated aboveground

49 carbon stocks (*19*). Then, to better assess the dynamic controls on aboveground carbon stocks, we

50 also computed the rate of carbon gained by the system (aboveground woody carbon production,

51 calculated as tree growth plus newly recruited trees, in Mg C ha^{-1} yr^{-1}), and its longevity in living

52 biomass (carbon residence time, calculated as the ratio of stocks to gains, in years).

53 We find considerable variation in biomass carbon among continents, with lower stocks per unit area

54 in South America compared with the Paleotropics even after accounting for environmental variables

55 (Fig. 1). Continents with high carbon stocks had either large carbon gains (Asia), or long carbon

56 residence times (Africa, Fig. 1). Because of these differences among continents, which are potentially

57 due to differences in evolutionary history (*20*), we analyse the environmental drivers of spatial

58 variation in carbon stocks while accounting for biogeographical differences. We fitted linear models

59 with explanatory variables representing hypothesised mechanistic controls of climate on tropical

60 forest carbon (Table S1). We also included soil covariates, continent intercepts and eigenvectors

61 describing spatial relationships amongst plots to account for other sources of variation (*21*).

62 Forest carbon stocks were most strongly related to maximum temperature (-5.9 % per 1°C increase in

63 maximum temperature, 95 % CI = -8.6 to -3.1 %, Fig. 2, equivalent to 9.1 Mg C ha^{-1} °C^{-1} for a stand

64 with the mean carbon stocks in our dataset, 154.6 Mg C ha^{-1}), followed by rainfall (+2.4 % per 100

65 mm increase in precipitation in the driest quarter, 95 % CI = 0.6 – 4.3 %, Fig. 2), with no statistically

66 significant relationship with minimum temperature, wind speed or cloud cover (Fig 2). The effects of

67 maximum temperature and precipitation are also evident in an analysis considering a wider suite of

9

68   climate variables than those tied to hypothesised mechanisms (Fig. S3), and in an additional

69   independent pantropical dataset of 223 single-census plots (for which carbon gains and residence time

70   cannot be assessed, Fig. S4).

71   The negative effect of maximum temperature on aboveground carbon stocks mainly reflects reduced

72   carbon gains in hotter forests (-4.0 % per 1°C, 95% CI = -6.2 to -1.8 %, Fig. 2) while the positive

73   effect of precipitation emerges through longer carbon residence times in wetter forests (3.3 % per 100

74   mm, 95 % CI = 0.9 – 5.7 %, Fig. 2). Carbon residence time also increased with the proportion of clay

75   in the soil (Fig. 2). The additive effects of precipitation and temperature on carbon stocks were

76   modified by an interaction between them (Δ AIC = 15.4 comparing full linear model with or without

77   interaction), with temperature effects more negative when precipitation is low (Fig. S6). The

78   interaction was through shortening carbon residence time (Δ AIC = 11.9) rather than reducing carbon

79   gains (model without interaction better, Δ AIC = 1.4).

80   An alternative analysis using decision tree algorithms (22) also showed maximum temperature and

81   precipitation to be important (Fig. S7). This decision tree approach, which can capture complex non-

82   linear relationships (22), indicated potential non-linearity in the relationships between carbon stocks

83   and both temperature and precipitation, with the positive effect of increasing dry season precipitation

84   on residence times strengthening when precipitation was low, and the negative effect of maximum

85   temperature intensifying at high temperatures (Fig. S7).

86   We further investigated non-linearity in the temperature relationship using breakpoint regression

87   (supported over linear regression based on lower AIC, Δ AIC = 15.0), which revealed that above 32.2

88   °C (95 % CI = 31.7 – 32.6 °C) the relationship between carbon stocks and maximum temperature

89   became more negative (cooler than breakpoint: -3.8 % °C^{-1}, warmer than breakpoint: -14.7 % °C^{-1},

90   Fig. 3). By partitioning carbon stocks into their production and persistence we find that this non-

91   linearity reflects changes to carbon residence time (Δ AIC = 10.6) rather than gains (Δ AIC = 1.7).

92   Overall, our results thus indicate two separate climate controls on carbon stocks: a negative linear

93   effect of maximum temperature through reduced carbon gains, and a non-linear negative effect of

94   maximum temperature, ameliorated by high dry-season precipitation, through reduced carbon

95   residence time.

96   The effect of temperature on carbon residence time only emerges when dry season precipitation is

97   low, so is consistent with theoretical expectations that negative effects of temperature on tree

98   longevity are exacerbated by moisture limitation rather than being independent of it (i.e. due to

99   increased respiration costs alone) (*23*). This could occur through high vapour pressure deficits in hot

100 and dry forests increasing mortality risk by causing hydraulic stress (*23, 24*), or carbon starvation due

101 to limited photosynthesis as a result of stomatal closure (*23*). Notably, the temperature-precipitation

102 interaction we find for aboveground stocks is in the opposite direction to temperature-precipitation

103 interactions reported for soil carbon. In soils, moisture limitation suppresses the temperature response

104 of heterotrophic respiration (*25*), while in trees moisture limitation enhances the mortality risks of

105 high temperatures.

106 The temperature effects on biomass carbon stocks and gains are primarily due to maximum rather

107 than minimum temperature. This is consistent with high daytime temperatures reducing CO_2

108 assimilation rates, for example due to increased photorespiration or longer duration of stomatal

109 closure (*26, 27*), whereas if negative temperature effects were to have increased respiration rates there

110 should be a stronger relationship with minimum (i.e. night-time) temperature. Critically, minimum

111 temperature is unrelated to aboveground carbon stocks both pan-tropically and in the one continent,

112 South America, where maximum and minimum temperature are largely decoupled ($r = 0.33$; Fig. S8).

113 While carbon gains are negatively related to minimum temperature (Fig S9) this bivariate relationship

114 is weaker than with maximum temperature, and disappears once the effects of other variables are

115 accounted for (Fig. 2). Finally, in Asia, the tropical region which experiences the warmest minimum

116 temperatures of all, both carbon stocks and carbon gains are highest (Fig. 1, Fig. S11).

117 Overall our results suggest that tropical forests have considerable potential to acclimate and adapt to

118 the effects of night-time minimum temperatures, but are clearly sensitive to the effects of daytime

119 maximum temperature. This is consistent with ecophysiological observations suggesting that the

120 acclimation potential of respiration (*15*) is greater than that of photosynthesis (*17*). The temperature

11

121   sensitivity revealed by our analysis is also considerably weaker than the short-term sensitivities

122   associated with inter-annual climate variation (*8*). For example, by relating short-term annual climate

123   anomalies to responses in plots, the effect of a 1°C increase in temperature on carbon gains has been

124   estimated as more than three-fold our long-term, pantropical result (*28*). This stronger long-term

125   thermal resilience is likely due to a combination of individual acclimation and plasticity (*15-17*),

126   differences in species' climate responses (*29*) leading to shifts in community composition due to

127   changing demographic rates (*12*) and the immigration of species with higher performance at high

128   temperatures (*12*).

129   Our pantropical analysis of the sensitivity to climate of aboveground carbon stocks, gains and

130   persistence shows that warming reduces carbon stocks and gains from woody productivity in tropical

131   forests. Using a reference carbon stock map (*30*) and applying our estimated temperature sensitivity

132   (including non-linearity) while holding other variables constant leads to a biome-wide reduction of

133   14.1 Pg C in live biomass (including scaling to estimate carbon in roots) for a 1°C increase in

134   maximum temperature (95 % CI = 6.9 – 20.7 Pg). In comparison, coupled climate-carbon cycle

135   models (*2*) give a median tropical land temperature sensitivity of 53 Pg C °C^{-1} (95 % CI = 19.7 – 86.3

136   Pg), although these also incorporate the response of heterotrophic respiration and fire. In the future,

137   reporting Earth System Model outputs for live biomass carbon separate from other changes would

138   assist in comparing model outcomes with direct observations.

139   Our results suggest that global surface temperature increases of 2°C above pre-industrial levels will

140   cause a potential biome-wide loss of 35.3 Pg C (95 % CI = 20.9 – 49.0 Pg) based on responses to

141   warming from the 1970-2000 baseline (*31*). The greatest reductions in carbon stocks are projected in

142   South America, where baseline temperatures and future warming are both highest (Fig. 4, Fig. S12).

143   This warming would push 71 % of the biome beyond the thermal threshold – maximum temperature

144   of 32.2°C – where larger reductions in biomass are expected. Of course, growth stimulation by carbon

145   dioxide (*32*) will partially or wholly offset the effect of this temperature increase, depending on both

146   the level of atmospheric carbon dioxide that limits warming to 2°C above pre-industrial levels and the

147   fertilization effect of this carbon dioxide on tropical trees. Using a variety of published estimates of

148   the carbon dioxide fertilization effect (Table S3), partial or full amelioration is expected in the

149   Paleotropics, although reductions in forest carbon stocks are predicted in South America in all

150   scenarios (Fig. S15).

151   The long-term climate sensitivities derived from our pan-tropical field measurements incorporate

152   ecophysiological and ecological adaptation, and so provide a model-independent estimate of the long-

153   term quasi-equilibrium response of tropical vegetation to climate, which can inform long-term model

154   predictions (*33*). We note that the thermal adaptation measured here may not be fully realised because

155   (i) the speed of temperature rises may exceed species' adaptive capabilities, (ii) habitat fragmentation

156   may limit species' ability to track changes in the environment, and (iii) other human impacts such as

157   logging and fire can increase the vulnerability of forest carbon stocks to high temperatures.

158   Predictions based on short-term inter-annual sensitivity and our long-term pan-tropical sensitivity

159   likely represent the upper and lower bounds of transient responses to rising temperatures over the

160   coming decades. While many tropical forests are under severe threat of conversion, our results show

161   that, in the long-run, tropical forests that remain intact can continue to store high levels of carbon

162   under high temperatures. Achieving the biome-wide climate resilience potential we document

163   depends on limiting heating and on large-scale conservation and restoration to protect biodiversity and

164   allow species to move.

165

166

References and Notes

1. P. M. Cox, R. A. Betts, C. D. Jones, S. A. Spall, I. J. Totterdell, Acceleration of global warming due to carbon-cycle feedbacks in a coupled climate model. *Nature* **408**, 184 (2000).

2. P. M. Cox *et al.*, Sensitivity of tropical carbon to climate change constrained by carbon dioxide variability. *Nature* **494**, 341-344 (2013).

3. B. B. B. Booth *et al.*, High sensitivity of future global warming to land carbon cycle processes. *Environmental Research Letters* **7**, 024002 (2012).

4. K.-H. Erb *et al.*, Unexpectedly large impact of forest management and grazing on global vegetation biomass. *Nature* **553**, 73 (2017).

5. W. Wang *et al.*, Variations in atmospheric CO_2 growth rates coupled with tropical temperature. *Proceedings of the National Academy of Sciences* **110**, 13061 (2013).

6. J. Liu *et al.*, Contrasting carbon cycle responses of the tropical continents to the 2015–2016 El Niño. *Science* **358**, eaam5690 (2017).

7. D. A. Clark, S. C. Piper, C. D. Keeling, D. B. Clark, Tropical rain forest tree growth and atmospheric carbon dynamics linked to interannual temperature variation during 1984–2000. *Proceedings of the National Academy of Sciences* **100**, 5852 (2003).

8. W. R. L. Anderegg *et al.*, Tropical nighttime warming as a dominant driver of variability in the terrestrial carbon sink. *Proceedings of the National Academy of Sciences* **112**, 15591-15596 (2015).

9. A. Ballantyne *et al.*, Accelerating net terrestrial carbon uptake during the warming hiatus due to reduced respiration. *Nature Climate Change* **7**, 148 (2017).

10. J. K. Green *et al.*, Large influence of soil moisture on long-term terrestrial carbon uptake. *Nature* **565**, 476-479 (2019).

11. O. L. Phillips *et al.*, Drought Sensitivity of the Amazon Rainforest. *Science* **323**, 1344 (2009).

191   12.   M. D. Smith, A. K. Knapp, S. L. Collins, A framework for assessing ecosystem dynamics in

192   response to chronic resource alterations induced by global change. *Ecology* **90**, 3279-3289

193   (2009).

194   13.   J. H. Brown, T. J. Valone, C. G. Curtin, Reorganization of an arid ecosystem in response to

195   recent climate change. *Proceedings of the National Academy of Sciences* **94**, 9729-9733

196   (1997).

197   14.   S. Fauset *et al.*, Drought-induced shifts in the floristic and functional composition of tropical

198   forests in Ghana. *Ecology Letters* **15**, 1120-1129 (2012).

199   15.   A. Gunderson Carla, H. O'Hara Keiran, M. Campion Christina, V. Walker Ashley, T. Edwards

200   Nelson, Thermal plasticity of photosynthesis: the role of acclimation in forest responses to a

201   warming climate. *Global Change Biology* **16**, 2272-2286 (2010).

202   16.   M. Slot *et al.*, Thermal acclimation of leaf respiration of tropical trees and lianas: response to

203   experimental canopy warming, and consequences for tropical forest carbon balance. *Global

204   Change Biology* **20**, 2915-2926 (2014).

205   17.   F. Ow Lai, L. Griffin Kevin, D. Whitehead, S. Walcroft Adrian, H. Turnbull Matthew, Thermal

206   acclimation of leaf respiration but not photosynthesis in Populus deltoides×nigra. *New

207   Phytologist* **178**, 123-134 (2008).

208   18.   T. F. Domingues *et al.*, Ecophysiological plasticity of Amazonian trees to long-term drought.

209   *Oecologia* **187**, 933-940 (2018).

210   19.   See suplimentary materials.

211   20.   J. W. F. Slik *et al.*, Phylogenetic classification of the world's tropical forests. *Proceedings of

212   the National Academy of Sciences* **115**, 1837 (2018).

213   21.   S. Dray, P. Legendre, P. R. Peres-Neto, Spatial modelling: a comprehensive framework for

214   principal coordinate analysis of neighbour matrices (PCNM). *Ecological Modelling* **196**, 483-

215   493 (2006).

216   22.   L. Breiman, Random Forests. *Machine Learning* **45**, 5-32 (2001).

15

217   23.   N. McDowell *et al.*, Drivers and mechanisms of tree mortality in moist tropical forests. *New*

218   *Phytologist* **219**, 851-869 (2018).

219   24.   G. Fontes Clarissa *et al.*, Dry and hot: the hydraulic consequences of a climate change–type

220   drought for Amazonian trees. *Philosophical Transactions of the Royal Society B: Biological*

221   *Sciences* **373**, 20180209 (2018).

222   25.   P. Ciais *et al.*, Europe-wide reduction in primary productivity caused by the heat and drought

223   in 2003. *Nature* **437**, 529-533 (2005).

224   26.   M. E. Dusenge, A. G. Duarte, D. A. Way, Plant carbon metabolism and climate change:

225   elevated CO_2 and temperature impacts on photosynthesis, photorespiration and respiration.

226   *New Phytologist* **221**, 32-49 (2019).

227   27.   S. Pau, M. Detto, Y. Kim, C. J. Still, Tropical forest temperature thresholds for gross primary

228   productivity. *Ecosphere* **9**, e02311 (2018).

229   28.   D. A. Clark, D. B. Clark, S. F. Oberbauer, Field-quantified responses of tropical rainforest

230   aboveground productivity to increasing CO_2 and climatic stress, 1997-2009. *Journal of*

231   *Geophyical Research - Biogeosciences.* **118**, 783-794 (2013).

232   29.   W. R. L. Anderegg *et al.*, Hydraulic diversity of forests regulates ecosystem resilience during

233   drought. *Nature* **561**, 538-541 (2018).

234   30.   V. Avitabile *et al.*, An integrated pan-tropical biomass map using multiple reference datasets.

235   *Global Change Biology* **22**, 1406-1420 (2016).

236   31.   S. E. Fick, R. J. Hijmans, WorldClim 2: new 1-km spatial resolution climate surfaces for global

237   land areas. *International Journal of Climatology* **37**, 4302-4315 (2017).

238   32.   S. Piao *et al.*, Evaluation of terrestrial carbon cycle models for their response to climate

239   variability and to CO_2 trends. *Global Change Biology* **19**, 2117-2132 (2013).

240   33.   L. M. Mercado *et al.*, Large sensitivity in land carbon storage due to geographical and

241   temporal variation in the thermal response of photosynthetic capacity. *New Phytologist* **218**,

242   1462-1477 (2018).

243   Additional references cited in suplementary materials

244   34.   A. B. Anderson, White-sand vegetation of Brazilian Amazonia. *Biotropica* **13**, 199-210 (1981).

245   35.   S. R. Pezeshki, Root responses of flood-tolerant and flood-sensitive tree species to soil redox

246   conditions. *Trees* **5**, 180-186 (1991).

247   36.   O. L. Phillips, T. R. Baker, T. R. Feldpausch, R. J. W. Brienen, *RAINFOR Field Manual for Plot*

248   *Establishment and Remeasurement* (University of Leeds, 2001).

249   37.   J. Talbot *et al.*, Methods to estimate aboveground wood productivity from long-term forest

250   inventory plots. *Forest Ecology and Management* **320**, 30-38 (2014).

251   38.   D. B. Clark, D. A. Clark, Landscape-scale variation in forest structure and biomass in a tropical

252   rain forest. *Forest Ecology and Management* **137**, 185-198 (2000).

253   39.   G. Lopez-Gonzalez, S. L. Lewis, M. Burkitt, O. L. Phillips, ForestPlots.net: a web application

254   and research tool to manage and analyse tropical forest plot data. *Journal of Vegetation*

255   *Science* **22**, 610-613 (2011).

256   40.   G. Lopez-Gonzalez, S. L. Lewis, M. Burkitt, T. R. Baker, O. L. Phillips, ForestPlots.net Database.

257   www.forestplots.net. (2009).

258   41.   R. J. W. Brienen *et al.*, Long-term decline of the Amazon carbon sink. *Nature* **519**, 344-348

259   (2015).

260   42.   J. Chave *et al.*, Improved allometric models to estimate the aboveground biomass of tropical

261   trees. *Global Change Biology* **20**, 3177-3190 (2014).

262   43.   J. Chave *et al.*, Towards a worldwide wood economics spectrum. *Ecology Letters* **12**, 351-366

263   (2009).

264   44.   A. E. Zanne *et al.* Data from: Towards a worldwide wood economics spectrum.

265   https://datadryad.org/stash/dataset/doi:10.5061/dryad.234 (Dryad Data Repository, 2009).

266   45.   R. C. Goodman *et al.*, Amazon palm biomass and allometry. *Forest Ecology and Management*

267   **310**, 994-1004 (2013).

17

268   46.   M. J. P. Sullivan *et al.*, Field methods for sampling tree height for tropical forest biomass

269   estimation. *Methods in Ecology and Evolution* **9**, 1179-1189 (2018).

270   47.   S. C. Thomas, Asymptotic height as a predictor of growth and allometric characteristics in

271   malaysian rain forest trees. *American Journal of Botany* **83**, 556-566 (1996).

272   48.   T. R. Feldpausch *et al.*, Tree height integrated into pantropical forest biomass estimates.

273   *Biogeosciences* **9**, 3381-3403 (2012).

274   49.   T. S. Kohyama, T. I. Kohyama, D. Sheil, Definition and estimation of vital rates from repeated

275   censuses: Choices, comparisons and bias corrections focusing on trees. *Methods in Ecology*

276   *and Evolution* **9**, 809-821 (2018).

277   50.   A. R. Martin, M. Doraisami, S. C. Thomas, Global patterns in wood carbon concentration

278   across the world's trees and forests. *Nature Geoscience* **11**, 915-920 (2018).

279   51.   D. Galbraith *et al.*, Residence times of woody biomass in tropical forests. *Plant Ecology &*

280   *Diversity* **6**, 139-157 (2013).

281   52.   G. Lopez-Gonzalez, M. J. P. Sullivan, T. R. Baker. BiomasaFP: R package for analysing data

282   downloaded from ForestPlots.net (2015).

283   53.   R. J. Hijmans, S. Phillips, J. Leathwick, J. Elith, dismo: Species distribution modeling. R

284   package version 1.0-12. (2015).

285   54.   A. M. Wilson, W. Jetz, Remotely Sensed High-Resolution Global Cloud Dynamics for

286   Predicting Ecosystem and Biodiversity Distributions. *PLOS Biology* **14**, e1002415 (2016).

287   55.   M. New, D. Lister, M. Hulme, I. Makin, A high-resolution data set of surface climate over

288   global land areas. *Climate Research* **21**, 1-25 (2002).

289   56.   T. Hengl *et al.*, SoilGrids250m: Global gridded soil information based on machine learning.

290   *PLOS ONE* **12**, e0169748 (2017).

291   57.   P. R. Peres-Neto, P. Legendre, Estimating and controlling for spatial structure in the study of

292   ecological communities. *Global Ecology and Biogeography* **19**, 174-184 (2010).

293 58. S. L. Lewis *et al.*, Increasing carbon storage in intact African tropical forests. *Nature* **457**,

294   1003 (2009).

295 59. K. Barton, MuMIn: Multi-Model Inference. R package version 1.12.1. http://CRAN.R-

296   project.org/package=MuMIn (2015).

297 60. V. M. R. Muggeo, Estimating regression models with unknown break-points. *Statistics in*

298   *Medicine* **22**, 3055-3071 (2003).

299 61. A. Liaw, M. Wiener, Classificiation and Regression by randomForest. *R News* **2**, 18-22 (2002).

300 62. D. M. Olson *et al.*, Terrestrial Ecoregions of the World: A New Map of Life on EarthA new

301   global map of terrestrial ecoregions provides an innovative tool for conserving biodiversity.

302   *BioScience* **51**, 933-938 (2001).

303 63. M. C. Hansen *et al.*, High-Resolution Global Maps of 21st-Century Forest Cover Change.

304   *Science* **342**, 850-853 (2013).

305 64. R. Jackson *et al.*, A global analysis of root distributions for terrestrial biomes. *Oecologia* **108**,

306   389-411 (1996).

307 65. S. S. Saatchi *et al.*, Benchmark map of forest carbon stocks in tropical regions across three

308   continents. *Proceedings of the National Academy of Sciences* **108**, 9899-9904 (2011).

309 66. A. Baccini *et al.*, Estimated carbon dioxide emissions from tropical deforestation improved

310   by carbon-density maps. *Nature Climate Change* **2**, 182-185 (2012).

311 67. E. T. A. Mitchard *et al.*, Uncertainty in the spatial distribution of tropical forest biomass: a

312   comparison of pan-tropical maps. *Carbon Balance and Management* **8**, 10 (2013).

313 68. E. T. Mitchard *et al.*, Markedly divergent estimates of A mazon forest carbon density from

314   ground plots and satellites. *Global Ecology and Biogeography* **23**, 935-946 (2014).

315 69. R. J. Hijmans. WorldClim Future Climate Data https://www.worldclim.org/cmip5v1. (2005).

316 70. R. J. Hijmans, S. E. Cameron, J. L. Parra, P. G. Jones, A. Jarvis, Very high resolution

317   interpolated climate surfaces for global land areas. *International Journal of Climatology* **25**,

318   1965-1978 (2005).

19

319   71.   B. Kirtman *et al.*, Near-term climate change: projections and predictability. (2013).

320   72.   H. D. Matthews, K. Caldeira, Stabilizing climate requires near-zero emissions. *Geophysical*

321   *Research Letters* **35**, (2008).

322   73.   M. Meinshausen *et al.*, The RCP greenhouse gas concentrations and their extensions from

323   1765 to 2300. *Climatic Change* **109**, 213 (2011).

324   74.   W. Kolby Smith *et al.*, Large divergence of satellite and Earth system model estimates of

325   global terrestrial CO2 fertilization. *Nature Climate Change* **6**, 306 (2015).

326   75.   D. W. Kicklighter *et al.*, A first-order analysis of the potential role of CO2 fertilization to affect

327   the global carbon budget: a comparison of four terrestrial biosphere models. *Tellus B:*

328   *Chemical and Physical Meteorology* **51**, 343-366 (1999).

329   76.   Y. Malhi *et al.*, The linkages between photosynthesis, productivity, growth and biomass in

330   lowland Amazonian forests. *Global Change Biology* **21**, 2283-2295 (2015).

331   77.   C. Terrer *et al.*, Nitrogen and phosphorus constrain the CO2 fertilization of global plant

332   biomass. *Nature Climate Change* **9**, 684-689 (2019).

333   78.   E. Bartholome, A. S. Belward, GLC2000: a new approach to global land cover mapping from

334   Earth observation data. *International Journal of Remote Sensing* **26**, 1959-1977 (2005).

335   79.   J. Chave *et al.*, Tree allometry and improved estimation of carbon stocks and balance in

336   tropical forests. *Oecologia* **145**, 87-99 (2005).

337   80.   M. Slot, K. Winter, In situ temperature response of photosynthesis of 42 tree and liana

338   species in the canopy of two Panamanian lowland tropical forests with contrasting rainfall

339   regimes. *New Phytologist* **214**, 1103-1117 (2017).

340   81.   Y. Malhi, The productivity, metabolism and carbon cycle of tropical forest vegetation.

341   *Journal of Ecology* **100**, 65-75 (2012).

342   82.   E. A. Graham, S. S. Mulkey, K. Kitajima, N. G. Phillips, S. J. Wright, Cloud cover limits net CO2

343   uptake and growth of a rainforest tree during tropical rainy seasons. *Proceedings of the*

344   *National Academy of Sciences* **100**, 572-576 (2003).

345   83.   W. F. Laurance, T. J. Curran, Impacts of wind disturbance on fragmented tropical forests: A

346   review and synthesis. *Austral Ecology* **33**, 399-408 (2008).

407

408 **Supplementary Materials:**

409 Materials and Methods

410 Figures S1-S15

411 Tables S1-S3

412 References (34-83)

413

414
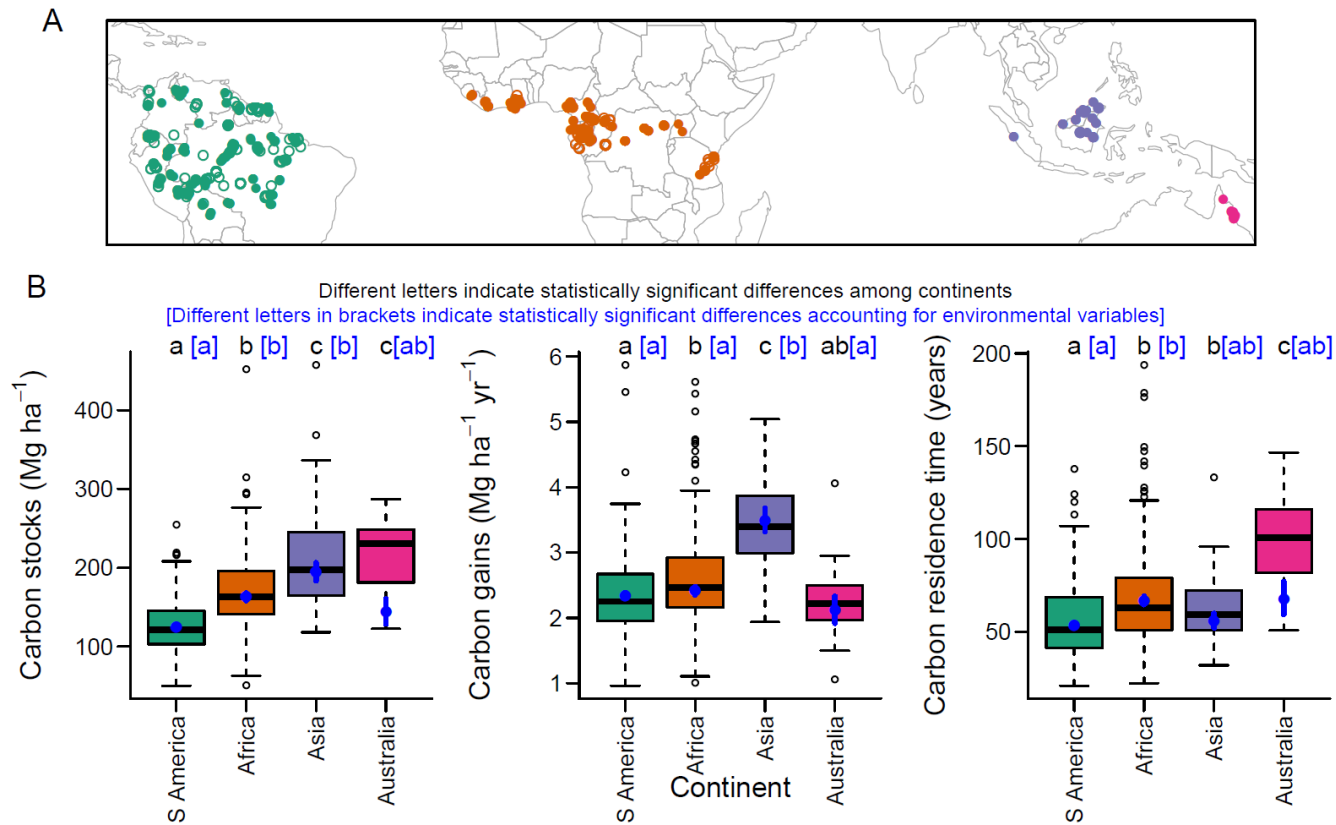
Figure 1. Spatial variation in tropical forest carbon. (A) Our plot network. Filled symbols show multi-census plots used in the main analysis, open symbols show single-census plots used as an independent dataset. (B) Variation in carbon among continents. Boxplots show raw variation while blue points show estimated mean values (± SE) after accounting for environmental variation. Letters denote statistically significant differences between continents (P < 0.05) based on raw data (black) or accounting for environmental effects (blue, square brackets).

24

419

420
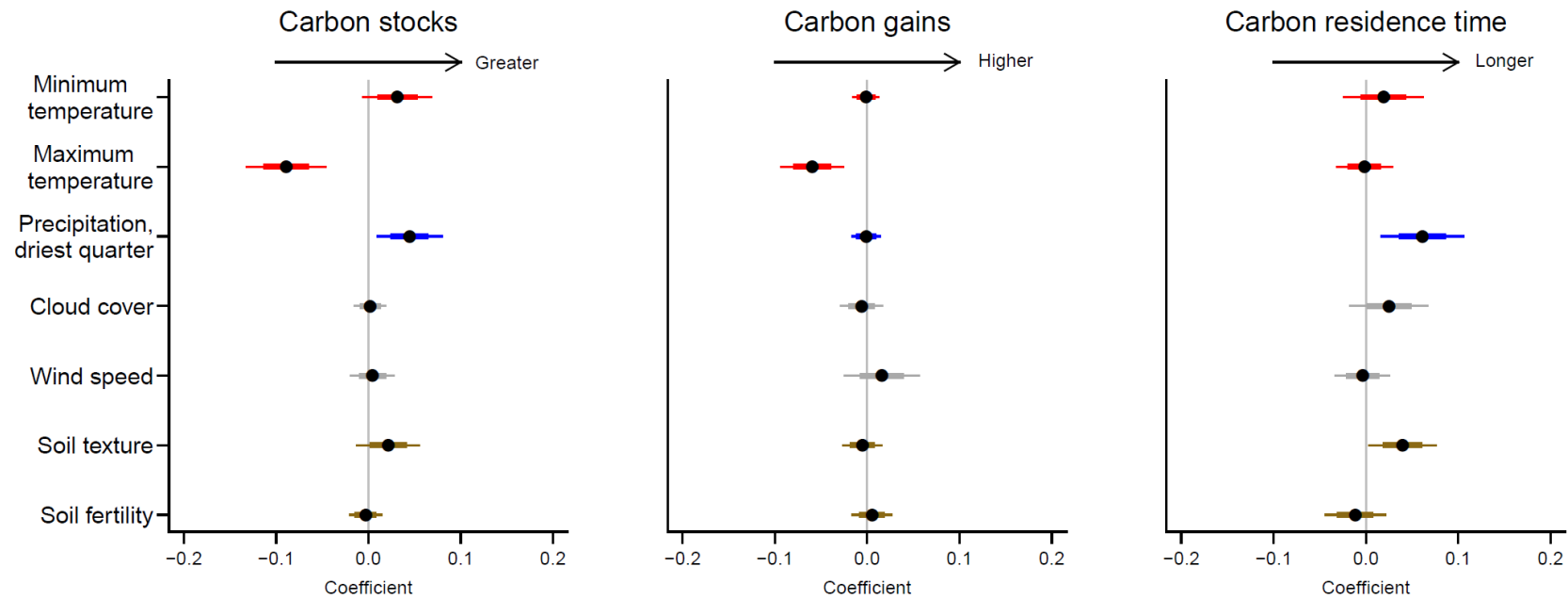
Figure 2. Correlates of spatial variation in tropical forest carbon. Points show coefficients from model-averaged general linear models. Variables that did not

occur in well-supported models are shrinkage adjusted towards zero. Coefficients are standardised so that they represent change in the response variable for

one standard deviation change in the explanatory variable. Error bars show standard errors (thick lines) and 95% confidence intervals (thin lines). Soil texture

is represented by the percentage clay, and soil fertility by cation exchange capacity. The full models explained 44.1 %, 31.4 % and 30.9 % of spatial variation

in carbon stocks, gains and residence time respectively. Coefficients are shown in Table S2. Results are robust to using an alternative allometry to estimate

tree biomass (Fig. S5).

427

428
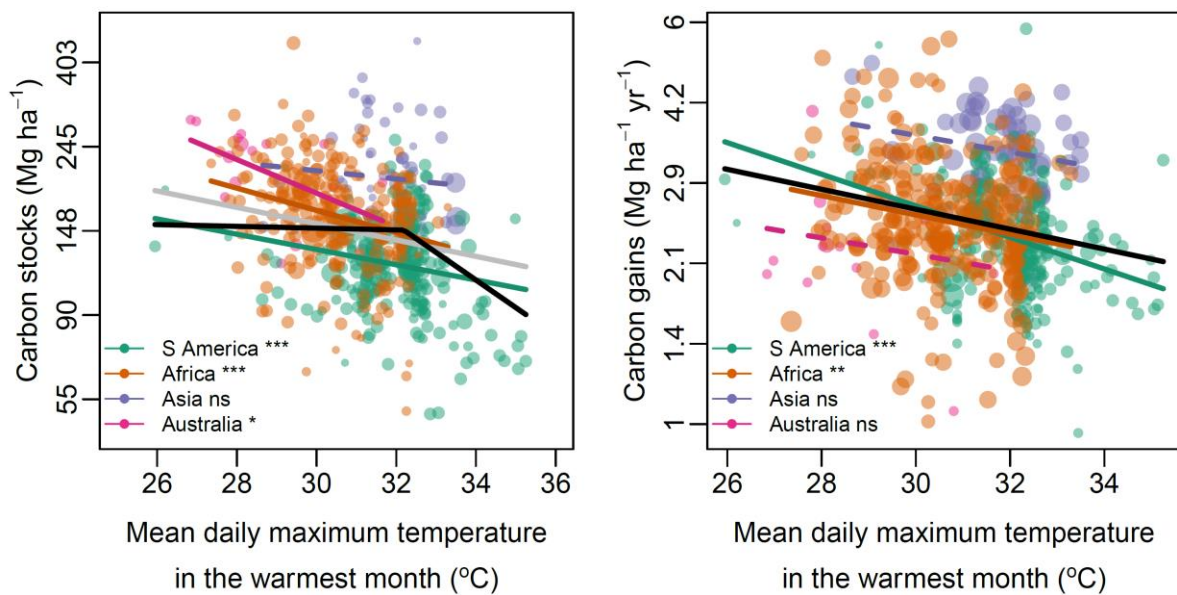
429

430

431 **Figure 3.** Temperature effects on tropical forest carbon stocks (left) and carbon gains from woody

432 productivity (right). Black lines show the best pan-tropical relationships accounting for environmental

433 covariates. The grey line shows the additional linear pan-tropical relationship for carbon stocks.

434 Coloured lines show bivariate relationships within each continent. Statistically significant

435 relationships are shown with solid lines, non-significant with dashed lines. Symbol point size is

436 proportional to weights used in model fitting based on plot size and monitoring length, see SI

437 Materials and Methods. Linear and break-point pan-tropical relationships are all statistically

438 significant ($P < 0.001$), as are better sampled continents. Relationships with other variables are shown

439 in Fig. S8-S10. *** $P < 0.001$, ** $P < 0.01$, * $P < 0.05$, ns $P \geq 0.05$.

440

441
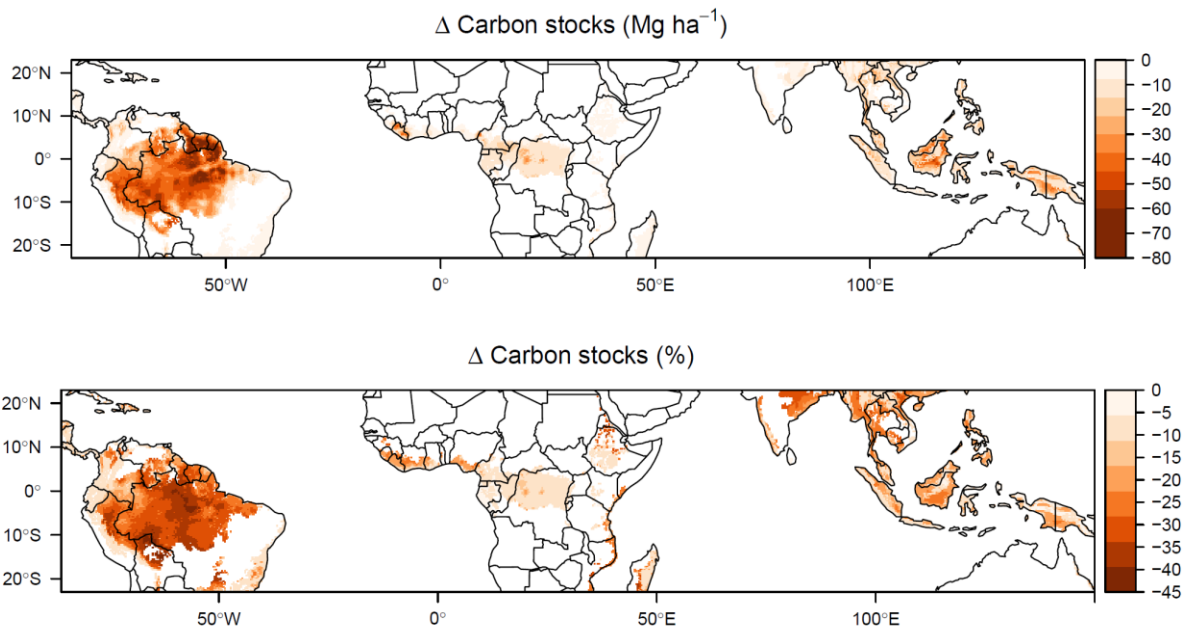
442

443 **Figure 4.** Long-term change in carbon stocks due to global surface temperature warming of

444 approximately 2°C. Future temperatures come from an ensemble of 15 climate models for RCP4.5,

445 2040-2060, which give global mean surface temperatures ~ 1.9°C above pre-industrial. Maps show

446 the predicted absolute and relative change in tropical forest carbon stocks if global temperatures

447 equilibrated at these new levels, based on the increase in maximum temperature from 1970-2000

448 baseline climate. Note parts of the biome become warmer than currently observed in our dataset (Fig.

449 S13). See Fig. S14 for predictions using alternative carbon reference maps. Predictions are based on

450 temperature alone and do not include precipitation changes (for which future patterns of change are

451 uncertain) or potential moderation via elevated CO_2 (see Fig. S15).

452

453

2

454   **Supporting information for Long-term thermal Sensitivity of the Earth's Tropical**
455   **Forests**

456   Martin J. P. Sullivan[1,2], Simon L. Lewis[1,3], Kofi Affum-Baffoe[4], Carolina Castilho[5], Flávia Costa[6], Aida
457   Cuni Sanchez[7,8], Corneille E. N. Ewango[9,10,11], Wannes Hubau[1,12,13], Beatriz Marimon[14], Abel Monteagudo-
458   Mendoza[15], Lan Qie[16], Bonaventure Sonké[17], Rodolfo Vasquez Martinez[15], Timothy R Baker[1], Roel J. W.
459   Brienen[1], Ted R. Feldpausch[18], David Galbraith[1], Manuel Gloor[1], Yadvinder Malhi[19], Shin-Ichiro Aiba[20],
460   Miguel N. Alexiades[21], Everton C. Almeida[22], Edmar Almeida de Oliveira[23], Esteban Álvarez Dávila[24],
461   Patricia Alvarez Loayza[25], Ana Andrade[26], Simone Aparecida Vieira[27], Luiz Aragão[28], Alejandro Araujo-
462   Murakami[29], Eric J.M.M. Arets[30], Luzmila Arroyo[31], Peter Ashton[32], Gerardo Aymard C.[33], Fabrício B.
463   Baccaro[34], Lindsay F. Banin[35], Christopher Baraloto[36], Plínio Barbosa Camargo[37], Jos Barlow[38], Jorcely
464   Barroso[39], Jean-François Bastin[40], Sarah A. Batterman[1,41,42,43], Hans Beeckman[12], Serge K. Begne[17,44], Amy
465   C. Bennett[44], Erika Berenguer[19,38], Nicholas Berry[45], Lilian Blanc[46], Pascal Boeckx[47], Jan Bogaert[48], Damien
466   Bonal[49], Frans Bongers[50], Matt Bradford[51], Francis Q. Brearley[2], Terry Brncic[52], Foster Brown[53], Benoit
467   Burban[54], José Luís Camargo[26], Wendeson Castro[55], Carlos Céron[56], Sabina Cerruto Ribeiro[57], Victor
468   Chama Moscoso[15], Jérôme Chave[58], Eric Chezeaux[59], Connie J. Clark[25], Fernanda Coelho[1], Murray
469   Collins[61], James A. Comiskey[62,63], Fernando Cornejo Valverde[64], Massiel Corrales Medina[65], Lola da
470   Costa[66], Martin Dančák[67], Greta C. Dargie[1], Stuart Davies[68], Nallaret Davila Cardozo[69], Thales de
471   Haulleville[12,48], Marcelo Brilhante de Medeiros[70], Jhon del Aguila Pasquel[71], Géraldine Derroire[72], Anthony
472   Di Fiore[73], Jean-Louis Doucet[74], Aurélie Dourdain[72], Vincent Droissant[75], Luisa Fernanda Duque[76], Romeo
473   Ekoungoulou[77], Fernando Elias[78], Terry Erwin[79], Adriane Esquivel-Muelbert[80], Sophie Fauset[81], Joice
474   Ferreira[82], Gerardo Flores Llampazo[83], Ernest Foli[84], Andrew Ford[51], Martin Gilpin[1], Jefferson S. Hall[85],
475   Keith C. Hamer[86], Alan C. Hamilton[87], David J. Harris[88], Terese B. Hart[89,90], Radim Hédl[91,92], Bruno
476   Herault[72], Rafael Herrera[93], Niro Higuchi[6], Annette Hladik[94], Eurídice Honorio Coronado[71], Isau
477   Huamantupa-Chuquimaco[95], Walter Huaraca Huasco[95], Kathryn J. Jeffery[96], Eliana Jimenez-Rojas[97],
478   Michelle Kalamandeen[1], Marie-Noel Kamdem[11,13,17,98], Elizabeth Kearsley[99], Ricardo Keichi Umetsu[100], Lip
479   Khoon Kho Khoon[101], Timothy Killeen[102], Kanehiro Kitayama[103], Bente Klitgaard[104], Nicolas Labrière[58],
480   William Laurance[105], Susan Laurance[105], Miguel E. Leal[106], Aurora Levesley[1], Adriano J. N. Lima[6], Janvier
481   Lisingo[11], Aline P. Lopes[107,108], Gabriela Lopez-Gonzalez[1], Tom Lovejoy[109], Jon Lovett[1], Richard Lowe[110],
482   William E. Magnusson[111], Jagoba Malumbres-Olarte[112,113], Ângelo Gilberto Manzatto[114], Ben Hur Marimon
483   Junior[115], Andrew R. Marshall[8,116,117], Toby Marthews[118], Simone Matias de Almeida Reis[14,19], Colin
484   Maycock[119], Karina Melgaço[1], Casimiro Mendoza[120], Faizah Metali[121], Vianet Mihindou[122,123], William
485   Milliken[104], Edward Mitchard[124], Paulo S. Morandi[14], Hannah L. Mossman[2], Laszlo Nagy[125], Henrique
486   Nascimento[6], David Neill[126], Reuben Nilus[127], Percy Núñez Vargas[95], Walter Palacios[128], Nadir Pallqui
487   Camacho[1,95], Julie Peacock[1], Colin Pendry[129], Maria Cristina Peñuela Mora[130], Georgia C. Pickavance[1], John
488   Pipoly[131], Nigel Pitman[132], Maureen Playfair[133], Lourens Poorter[134], John R. Poulsen[25], Axel D. Poulsen[135],
489   Richard Preziosi[2], Adriana Prieto[136], Richard Primack[137], Hirma Ramírez-Angulo[138], Jan Reitsma[139],
490   Maxime Réjou-Méchain[75], Zorayda Restrepo Correa[140], Thaiane Rodrigues de Sousa[6], Lily Rodriguez
491   Bayona[141], Anand Roopsind[142], Agustín Rudas[136], Ervan Rutishauser[42,143], Kamariah Abu Salim[121], Rafael
492   P. Salomão[144,145], Juliana Schietti[6], Douglas Sheil[146], Richarlly C. Silva[57,147], Javier Silva Espejo[148], Camila
493   Silva Valeria[38], Marcos Silveira[57], Murielle Simo-Droissart[17], Marcelo Fragomeni Simon[70], James Singh[149],
494   Yahn Carlos Soto Shareva[15], Clement Stahl[54], Juliana Stropp[150], Rahayu Sukri[121], Terry Sunderland[151,152],
495   Martin Svátek[153], Michael D. Swaine[154], Varun Swamy[155], Hermann Taedoumg[17], Joey Talbot[1], James
496   Taplin[156], David Taylor[157], Hans ter Steege[158,159], John Terborgh[25], Raquel Thomas[142], Sean C. Thomas[160],
497   Armando Torres-Lezama[161], Peter Umunay[162,163], Luis Valenzuela Gamarra[15], Geertje van der Heijden[164],
498   Peter van der Hout[165], Peter van der Meer[166], Mark van Nieuwstadt[167], Hans Verbeeck[99], Ronald
499   Vernimmen[168], Alberto Vicentini[6], Ima Célia Guimarães Vieira[145], Emilio Vilanova Torre[169], Jason
500   Vleminckx[36], Vincent Vos[171], Ophelia Wang[172], Lee J. T. White[123,173,174], Simon Willcock[175], John T.
501   Woods[176], Verginia Wortel[177], Kenneth Young[178], Roderick Zagt[179], Lise Zemagho[17], Pieter A. Zuidema[50],
502   Joeri A. Zwerts[177,180], Oliver L. Phillips[1]

503

504

3

Supporting information for Sullivan et al.

505 **This file includes:**

506 Materials and Methods

507 Figures S1 – S15

508 Tables S1 – S3

509

4

Materials and Methods

<u>Forest census data</u>

510
511
512 Our plots come from the RAINFOR, AfriTRON, and T-FORCES networks. Forest inventory plots

513 were located in lowland (<1200 m), old-growth, closed-canopy forests that were not known to have

514 been subject to anthropogenic disturbance through fire or selective logging. Plots characterised

515 floristically as dry forest were not included, as were plots that received less than 1200 mm

516 precipitation each year. We also did not include plots in white sand, swamp and seasonally flooded

517 forests, as we expect these to experience marked edaphic constraints (extreme nutrient limitation for

518 white sand forests (*34*), stress caused by hypoxic conditions for swamp and seasonally flooded forests

519 (*35*)). All plots were ≥ 0.2 ha (median size = 1 ha) and were monitored for at least two years (median

520 monitoring period = 9.7 years). All censuses were prior to the 2015-16 very strong El Niño event, as

521 we expected that event to supress carbon gains relative to the long-term mean.

522 Forest inventory plots were sampled using standardised protocols (*36*), where all live stems with

523 diameter ≥ 100 mm were measured at 1.3 m or 50 cm above buttresses and deformities. Trees were

524 tagged so that the same tree could be identified in subsequent censuses. In some cases the point of

525 diameter measurement (POM) had to be moved due to upward growth of buttresses and deformities.

526 For these trees we use the D_{mean} approach from Talbot et al. (*37*).

527 In a few cases (6 plots) the minimum diameter measured changed over time, or palms and

528 *Phenakospermum* were excluded in some censuses. For these, we estimated aboveground biomass

529 (AGB, subsequently converted to carbon stocks) and aboveground woody production (AGWP,

530 subsequently converted to carbon gains) using a minimum diameter or taxonomic protocol that could

531 be consistently applied across censuses, and scaled these values by the aboveground biomass ratio

532 between that protocol and all stems ≥ 100 mm protocol for censuses when all stems were measured.

533 Some plots had nested designs where the plot was split into subplots with different minimum diameter

534 protocols (69 plots). For these, we only analysed the area conforming to our minimum diameter

535 protocol. For analysis, we grouped small (≤ 0.5 ha) plots within 1 km of each other, and also grouped

5

536   contiguous larger plots (18 plots), as these will experience equivalent climate and larger plots are less

537   sensitive to stochastic tree fall events (*38*).

538   Data were curated in ForestPlots.net (*39, 40*), or were subject to equivalent offline handling, and

539   experienced the same quality control procedures. Details of quality control procedures are described

540   in Brienen et al. (*41*). Our final dataset consists of 590 sampling units (hereafter plots) covering 637.2

541   ha, with 2.2 million measurements of 670,499 unique stems. For validating models of carbon stocks

542   an additional dataset of 223 single-census plots using the same measurement protocols was assembled

543   from the same networks (see section "Validation with independent single-census plot dataset" below).

544

545   <u>Estimating above-ground biomass</u>

546   Diameter measurements were converted to estimates of aboveground biomass (AGB). For dicot trees

547   we used the allometric equation

548     $\text{AGB} = 0.673 \times (\rho D^2 H)^{0.976}$,   [1]

549   from Chave et al. (*42*), where ρ is wood density (from (*43, 44*)) and H is tree height estimated using

550   allometric equations described below. For monocots and tree ferns, we used a palm-specific

551   allometric equation

552     $\ln(\text{AGB}) = -3.3488 + 2.7483.\ln(D)$,   [2]

553   from Goodman et al. (*45*), where D is the measured diameter.

554   The heights of a subset of trees in our dataset were measured in the field, either with a laser

555   rangefinder, hypsometer, or clinometer, or directly by climbing the tree. We filtered this dataset to

556   stems with measured diameters, height $\leq$ 90 m, diameters $\geq$ 90 mm DBH, as height-diameter

557   allometries of saplings differ from those of more mature trees, and to stems that were not broken,

558   leaning or fallen. This gave a total of 78,899 height measurements. We used this dataset to fit local

559   height-diameter allometric models, as these refine AGB estimates by capturing spatial variation in

560   height-diameter allometries missed by large-scale allometric models (*46*). Height data were not

6

561   available from every plot, so to ensure consistent treatment of plots height-diameter models were

562   constructed for each biogeographic region. We fitted three parameter asymptotic models (*47*) of the

563   form

564    $H = a(1-\exp(-bD^C))$,   [3]

565   where *a*, *b* and *c* are estimated parameters ('Weibull' models, *48*). We fitted these models either

566   treating each observation equally or with case weights proportional to each trees' basal area. These

567   weights give more importance to large trees during model fitting. We selected the best fitting of these

568   models, determining this as the model that minimised prediction error of stand biomass when

569   calculated with estimated heights or observed heights (*46*). Weibull models were implemented using

570   the nls function in R with default settings. Starting values of $a = 25$, $b = 0.05$ and $c = 0.7$ were chosen

571   following trial and error as they led to regular model convergence. Where models did not converge

572   this was usually because the height-diameter relationship did not reach an asymptote, so in these cases

573   we used the log-log model $\ln(H) = a + b(\ln(D))$ to estimate height, where *b* gives the scaling exponent

574   of a power law relationship between height and diameter. We checked if models gave unrealistic

575   predictions by applying models to predict the height of all trees in the biogeographic region, and

576   excluded models that predicted any tree height 10 % higher than the tallest tree we recorded in that

577   continent.

578

579   <u>Estimating above-ground woody production</u>

580   We estimated AGWP following Talbot et al. (*37*). AGWP is comprised of four components, (1) the

581   sum of growth of surviving trees, (2) the sum of AGB of new recruits, (3) the sum of unobserved

582   growth of trees that died during a census interval and (4) the sum of growth of unobserved recruits

583   that entered then died during a census interval. Accounting for the latter two components is necessary

584   to avoid census-interval length effects, as more AGWP in these components will be missed due to the

585   greater mortality of trees that accumulates over longer census intervals.

7

586   Components 3 and 4 can be estimated using two quantities that can be calculated from observed stem-

587   dynamics in each plot; per-area annual recruitment (R_a) and per-capita annual mortality (m_a). Per-

588   capita mortality is calculated from the ratio of surviving stems to initial stems, using equation 5 in

589   Kohyama et al. (*49*). Per-area annual recruitment is calculated using estimated mortality rates and the

590   observed change in the number of stems over a census interval, using equation 11 of Kohyama et al.

591   (*49*).

592   To estimate the unobserved growth of stems that died during a census interval, we first use plot-level

593   per-capita mortality rates (m_a) to estimate how many trees are expected to have died in each year of

594   the census interval, and from that calculate the mean number of years that trees that died during the

595   census interval would have lived before death. The diameter of tree at death (D_{death}) can then be

596   estimated as

597    $$D_{death} = D_{start} \times G \times Y_{mean} \qquad\qquad [4]$$

598   where D_{start} is the diameter at the start of the census interval, G is the plot-level median growth rate of

599   the size class the tree was in at the start of the census interval (size classes are defined as $D < 200$ mm,

600   400 mm $> D \geq 200$ mm, and $D \geq 400$ mm) and Y_{mean} is the mean number of years trees survived in

601   the census interval before dying. The diameter at death is then converted to AGB at death using

602   allometric equations (equation 1, except for ferns and monocots where equation 2 is used), and the

603   unobserved growth is calculated as the difference between AGB at death and AGB at the start of the

604   census.

605   To estimate the growth of recruits that were not observed because they died during the census

606   interval, we first need to estimate the number of unobserved recruits. This can be estimated from per-

607   area annual recruitment (R_a) and per-capita annual mortality (m_a): R_a gives the number of stems per ha

608   that recruit in a given year, and the probability of each recruit surviving until the next census (P_{surv}) is

609    $P_{surv} = (1-m_a)^T$, where T is the number of years remaining in the census interval. The number of

610   recruits in a given year that survive to the next census is $R_a - P_{surv}R_a$. Summing this for each year in a

611   census interval gives the total number of unobserved recruits in that census interval. We then need to

8

612   estimate how long each recruit was alive for. From m_a we can calculate the number of recruits in a

613   given year that died in each subsequent year, and from this calculate the mean life-span of recruits in a

614   given year that died before the next census. The average life-span of unobserved recruits ($Y_{mean-rec}$) is

615   the weighted mean of each cohort's lifespan, weighted by the number of unobserved recruits in each

616   year. Diameter at death is given in mm by

617    $D_{death} = 100 + (G \times Y_{mean-rec})$ [5]

618   where G is the plot-level median growth rate of the smallest size class (i.e. $D < 200$ mm).

619   Aboveground biomass of recruits at the time of death is estimated using equation 1. These corrections

620   for unobserved growth have a marginal impact on AGWP calculations, collectively accounting on

621   average for just 2.3 % of estimated plot-level AGWP.

622   AGB was calculated for each census, and AGWP was calculated for each census interval, and the

623   time-weighted mean of each was taken to give one value per plot. We used a time-weighted mean to

624   give greater importance to AGB estimates separated by longer census-intervals, as these will be more

625   independent. Estimates of AGB and AGWP were converted to carbon stocks and carbon gains by

626   multiplying by 0.456 (*50*). Carbon residence time was then estimated as carbon stocks /carbon gains,

627   and represents the length of time carbon resides in living biomass before being passed to the litter and

628   necromass pools (*51*). Calculations to estimate AGB and AGWP were performed using the R package

629   BiomasaFP (*52*).

630

631   <u>Obtaining environmental data</u>

632   Most climate data were obtained from climate data from Worldclim2 (*31*) as it provides the highest

633   resolution (~ 1 km) pantropical climate data, although we note that some regions, such as central

634   Africa, have limited station data. We extracted monthly data for the following variables: mean daily

635   minimum temperature, mean daily maximum temperature, precipitation, solar radiation and wind

636   speed, In addition to calculating the standard series of 19 bioclimatic variables, using the dismo R

637   package (*53*), we calculated 1) mean daily maximum temperature, BIO1 + BIO2/2, 2) mean daily

9

638   minimum temperature, BIO1 – BIO2/2, 3) maximum cumulative water deficit as the minimum across

639   the year of monthly cumulative water deficit W,

640    $W_i = W_{i-1} - \min(0, P_i - 100)$,   [6]

641   where P is monthly precipitation in mm, and 100 represents measured evapotranspiration. This

642   calculation was run for a year from the wettest month in the year, starting at a water deficit of zero, 4)

643   the number of months where monthly cumulative water deficit was negative, 5) the number of months

644   where monthly precipitation was below 100 mm (i.e. less than evapotranspiration), 6) mean annual

645   solar radiation, 7) mean annual wind speed, and 8) vapour pressure deficit (VPD = SVP – vapour

646   pressure, where saturated vapour pressure, SVP, $= 0.611 \times e^{(17.502\, temperature) / (temperature + 240.97)}$). We also

647   obtained data on cloud frequency at ~1 km resolution from Wilson & Jetz (*54*), who processed twice-

648   daily MODIS satellite images. Temperature values were adjusted for differences in altitude between

649   the plot and the 1 km grid cell used for Worldclim interpolation, as these can differ in topographically

650   diverse regions, using lapse rates, so that $T_{plot} = T_{worldclim} + 0.005 \times (A_{worldclim} - A_{plot})$, where T is

651   temperature (°C) and A is altitude (m). Temperature values were also corrected for systematic

652   warming trends. To do this, the mean annual temperature in each grid-cell in each year was extracted

653   from the CRU TS 3.24 dataset (*55*), and robust linear regression used to estimate grid-cell specific

654   warming rates. These were used to adjust Worldclim2 temperature values for the difference between

655   the midpoint of plot monitoring and the midpoint of the Worldclim2 climatology.

656   Data on soil texture and chemistry was obtained at 1 km resolution from the SoilGrids dataset (*56*),

657   with this resolution selected to match the resolution of the climate data. From this we extracted CEC,

658   representing soil fertility, and percentage clay, representing soil texture. For each soil variable we

659   calculated the depth-weighted average for 0 – 30 cm.

660   Statistical analysis

661   We used linear models to relate carbon, carbon gains and carbon residence time to environmental

662   explanatory variables. The role of different explanatory variables was assessed using multi-model

663   inference.

664   Response variables were positively skewed and had positive mean-variance relationships, so were

665   log-transformed to meet the assumption of normality and reduce heterogeneity in variances. The log-

666   normal nature of forest carbon stocks and dynamics means that there is greater potential for variation

667   when forests are large, which could be due to the non-linear scaling of tree biomass and tree basal

668   area.

669   We selected explanatory variables to represent hypothesised ways in which climate could affect

670   carbon stocks (Table S1). We assessed colinearity within this set of explanatory variables using

671   variance inflation factors (VIF) and pairwise correlations. Because of colinearity, we had to exclude

672   VPD, total precipitation, use only one of MCWD and precipitation in the driest quarter, and could

673   include both minimum and maximum temperature but not mean annual temperature. We used

674   precipitation in the driest quarter rather than MCWD as the latter is zero truncated and so is less

675   amenable to regression analysis. After removing these variables all pairwise correlations (including

676   with soil explanatory variables) were weak enough not to cause problems through collinearity ($r < 0.6$

677   and $VIF < 3$).

678   To account for variation other than in climate we also included soil variables relating to texture (%

679   clay) and fertility (CEC), and included continent specific intercepts to account for biogeographic

680   variation in carbon. To account for unmeasured environmental gradients (e.g. soil variation not

681   captured by the SoilGrids variables), we used Moran's eigenvector maps as explanatory variables,

682   selecting eigenvectors the corresponded to positive spatial autocorrelation in the distance matrix (*57*).

683   These variables act as a proxy for unmeasured spatial gradients by capturing positive spatial

684   associations between plots.

685   Plots differed in their area and the length of time they were monitored for. This is likely to affect the

686   variance of carbon stocks, carbon gains and carbon residence time, as smaller plots or plots only

687   monitored for short periods are more likely to be sensitive to the mortality of a few large trees. To

688   account for this, we used case weights relating to plot area and monitoring period. Following Lewis et

689   al. (*58*), we selected weights by relating residuals from our linear models to plot area and to plot

690   monitoring period, and subsequently assessing which root transformation of plot area/ monitoring

11

691   period removed the pattern in the residuals when used as a weight. Selected weights were: carbon

692   stocks, Area $^{1/3}$; carbon gains, Monitoring length $^{1/7}$; carbon residence time, Area $^{1/9}$ + Monitoring

693   length $^{1/12}$ -1.

694   We fitted all subsets of the general linear model with explanatory variables described above, forcing

695   spatial eigenvectors into all models. We then averaged the subset of models where Δ AIC < 4, using

696   full averaging so variables that do not appear in the model get the value of zero for their coefficients.

697   This means that model averaged coefficients of terms with limited support exhibit shrinkage towards

698   zero. Multi-model inference was performed using the MuMIn R package (*59*).

699   We assessed whether the two climate variables found to have important additive effects on carbon

700   stocks in this analysis (mean daily maximum temperature in the warmest month and precipitation in

701   the driest quarter) interacted with each other by adding an interaction term between these variables to

702   the full generalised linear model of carbon stocks as a function of other climate and soil variables,

703   continent and spatial eigenvectors. We compared these two models using AIC. We repeated this with

704   carbon gains and carbon residence time as response variables.

705   To assess whether the temperature carbon relationship was non-linear we used breakpoint regression

706   implemented in the segmented R package (*60*). This estimates a breakpoint in the explanatory variable

707   at which the slope of the relationship with the response variable changes. We estimated the breakpoint

708   for the mean daily maximum temperature in the warmest month variable in the full model with a

709   temperature-precipitation interaction described above. We assessed the support for the breakpoint by

710   comparing the AIC of the model with a breakpoint with the AIC of a model with a linear relationship.

711   We repeated this with carbon gains and carbon residence time as response variables.

712   We also analysed spatial variation in carbon stocks as a function of the above climate and soil

713   variables and spatial eigenvectors using Random Forest decision tree algorithms (*22*) implemented

714   using the randomForest R package (*61*). We assessed variable importance by calculating the average

715   increase in node purity across all decision trees (measured by residual sum of squares) when using the

716   variable to split the data. We assessed modelled relationships between response and explanatory

717 variables using partial plots, which show predicted change in the response variable, averaged across

718 trees, when changing the explanatory variable and holding all other variables constant.

719 To compliment this analysis based on relationships expected *a priori*, we also performed an

720 exploratory analysis to assess whether other climate variables excluded from the full general linear

721 models had an effect on carbon. To do this, we fitted linear models to assess the bivariate relationship

722 of carbon with each climate variable, with continent also included as an explanatory variable to

723 account for biogeographic variation in forest characteristics.

724

725 <u>Validation with independent single-census plot dataset</u>

726 We assessed whether the relationships with environmental variables identified in the analyses of

727 multi-census plot data described above held when applied to an additional dataset of 223 single-

728 census plots. As the single-census data were not used in any of the analyses above they did not

729 influence modelling decisions, so provide an independent test of the relationships identified with the

730 multi-census plot analysis.

731 Single-census plots were extracted from the ForestPlots.net database (*39, 40*) using the same plot-

732 selection criteria as for the multi-census plots, except that censuses during or following the 2015-16

733 strong El Niño were included in the single-census plot dataset as we expected that carbon stocks,

734 unlike gains, would still remain close to their long-term mean.

735 We fitted a general linear model with the five climate explanatory variables, soil fertility and texture,

736 continent and spatial eigenvector, and model averaging of all subsets of this model as described for

737 the multi-census plots. We performed this analysis using just the single-census plots and a combined

738 dataset of single and multi-census plots.

739

740 <u>Scaling results to the biome</u>

13

741   We applied the relationship between carbon stocks and mean daily maximum temperature in the

742   warmest month identified by the breakpoint regression to estimate the total change in carbon stock

743   due to temperature effects alone for different scenarios of temperature increase. We delimited the

744   biome extent using the WWF tropical and subtropical moist broadleaved forest biome (*62*), restricted

745   to tropical latitudes, and further refined it by excluding grid-cells with < 50 Mg C ha^{-1} using data from

746   (*30*), as these are unlikely to be forest. Calculations were conducted at 10-minute resolution. For each

747   grid-cell we predicted the percentage change in carbon for a given temperature increase from our

748   statistical model, holding all other variables constant. We then used a reference carbon stock map (*30*)

749   to convert percentage change to change in carbon stocks per hectare (in Mg ha^{-1}). To calculate change

750   in carbon stocks for the whole grid-cell, we multiplied change per hectare by the area of the grid-cell

751   in hectares, and then adjusted this by the proportion of the grid-cell that was forested by multiplying

752   by 2014 forest cover (*63*). Total change for the biome (in Pg) was calculated by summing these grid-

753   cell level values. Uncertainty due to our statistical model was assessed by generating multiple

754   predictions by resampling model parameters (breakpoint threshold, slope below breakpoint, slope

755   above breakpoint), and extracting quantiles from the resultant distribution of predicted change values.

756   Aboveground biomass carbon values were scaled to include root biomass based on a root to shoot

757   ratio of 0.19 in tropical evergreen forests (*64*).

758   The Avitabile et al (*30*) aboveground biomass map was chosen to provide reference carbon stocks.

759   While other maps have previously been produced by Saatchi et al. (*65*) and Baccini et al. (*66*) we

760   selected the Avitabile map because it synthesises the earlier maps (see Mitchard et al. (*67*) for

761   discussion of substantial differences between these maps) and is anchored by more field data.

762   Importantly, the Avitabile map reproduces spatial patterns in aboveground biomass that have been

763   described from field data but are absent in the Saatchi or Baccini maps, including the much higher

764   biomass density of north-east Amazonian forests due to tall trees and very high wood density (*68*).

765   Nevertheless, we also investigated the consequences of using the Saatchi or Baccini maps for our

766   estimates of biomewide thermal sensitivity and spatial patterns of change in carbon stocks (Fig S15).

14

767   We investigated three temperature change scenarios. Firstly, we applied a 1°C increase to all

768   locations. Secondly, we assessed the consequence of a 1.5°C increase in global temperature from pre-

769   industrial levels for the equilibrium temperature response of tropical forest carbon. Finally, we

770   assessed the consequence of a 2°C increase in global temperature from pre-industrial levels. For the

771   latter two we obtained data from CMIP5 climate models, using downscaled future climate projections

772   based on the Worldclim climatology (*69*). As downscaling was performed using Worldclim version

773   1.4 (*70*) and our statistical models use Worldclim version 2, we calculated the warming anomaly in

774   each grid-cell from the current Worldclim version 1.4 conditions, and applied this to the Worldclim 2

775   data to obtain future temperature. RCP scenarios and time-points were chosen to give global

776   temperature increases that best match 1.5°C and 2°C above pre-industrial. For 1.5°C we used RCP 2.6

777   averaged for 2040-2060 (median temperature increase across models = 1.5°C, (*71*)). For 2°C, we used

778   RCP 2.6 averaged for 2040-2060 (median temperature increase models = 1.9°C (*71*)). Note that

779   predicted increases in maximum temperatures were often considerably greater than the global

780   increase, especially in South America. For both scenarios we used the median predicted temperature

781   change for each grid-cell from an ensemble of 15 models (BCC-CSM1-1, CCSM4, CNRM-CM5,

782   GFDL-CM3, GFDL-ESM2G, GISS-E2-R, HadGEM2-AO, HadGEM-ES, IPSL-CM5A-LR, MIROC-

783   ESM-CHEM, MIROC-ESM, MIROC5, MPI-ESM-LR, MRI-CGCM3, NorESM1-M).

784   We assessed the potential for long-term carbon dioxide growth stimulation to offset these long-term

785   temperature effects. We used CO_2 concentrations from the RCP scenarios and time-points described

786   above, which approximate the long-term concentrations if the climate stabilised at the new

787   temperatures (*72*). Thus the 1.5°C and 2°C scenarios were associated with CO_2 concentrations of 443

788   ppm and 487 ppm respectively (*73*). We cannot assess the effect of CO_2 on biomass from our spatial

789   dataset, so instead used independent estimates of CO_2 effects from other sources. Firstly, we obtained

790   CO_2 only effects on net primary production (NPP) extracted from an ensemble of CMIP5 earth system

791   models by (*74*). This gives the proportional change in NPP for evergreen forests (note that this also

792   includes boreal forests) over 1980-2010, standardised to a 100 ppm increase in CO_2 concentration. To

793   propagate this through to changes in AGB under future CO_2 conditions we first estimated the

794   logarithmic dependency of NPP on CO_2 (75) by substituting values of NPP and CO_2 at time zero and t

795   (from (74)) into the equation,

796    $$NPP_t = NPP_0 \left[1 + \beta \ln \left(\frac{\lfloor CO_2 \rfloor_t}{\lceil CO_2 \rceil_0} \right) \right]$$ [7]

797   This equation can be used to compute NPP annually given an initial NPP estimate and a time series of

798   atmospheric CO_2 concentrations (from a combination of the observed record from pre-industrial and

799   the RCP 4.5 scenario, modified so that it stabilises at 487 or 443 ppm depending on warming

800   scenario). Initial pre-industrial NPP was back-calculated from present-day values using Equation 7,

801   with 13.3 Mg C ha^{-1} yr^{-1} (mean of nine Amazon plots where NPP has been measured, from (76)) used

802   for present-day NPP. To propagate NPP into change in woody biomass (following (51)) we used the

803   equation

804    $$\frac{dM_{\text{wood}}}{dt} = \alpha_{\text{wood}} N_P - \frac{M_{\text{wood}}}{\tau_{\text{wood}}}$$ [8]

805   where M_{wood} is woody biomass, N_p is NPP, α_{wood} is the allocation of NPP to wood (taken as 0.33, the

806   mean value across nine plots from (76)) and τ_{wood} is the residence time of woody biomass, taken as

807   59.1 years (the median value across plots used in this study). This model (equations 7 and 8) was run

808   from pre-industrial to 2500, enabling us to see the equilibrium effect of increased CO_2 concentrations

809   on biomass, assuming temporally invariant allocation and residence time. We calculated the

810   proportional change in biomass from 2000 to 2500, and applied this to the reference carbon stock map

811   to obtain predicted equilibrium change in aboveground biomass due to CO_2 effects.

812   The effects of CO_2 in earth system models have been reported to be larger than those deduced from

813   satellite data or CO_2 enrichment experiments (74), so we also ran the above model using changes in

814   NPP reported from a synthesis of free-air CO_2 enrichment experiments conducted in forests (74).

815   Finally, we looked at the impact of using CO_2 effects derived from a recent large meta-analysis of

816   CO_2 enrichment experiments (77), which reported a 12.5 % increase in biomass of tropical trees for a

817   250 ppm increase in CO_2 concentration. As this relationship was reported to be linear (77) we used

818   linear interpolation to estimate the change in biomass under CO_2 concentrations associated with each

16

819   warming scenario (i.e. 443 and 487 ppm). To estimate long-term changes in biomass accounting for

820   both temperature and carbon dioxide, we first applied the CO_2 relationship to estimate the change in

821   biomass due to carbon dioxide growth stimulation, and then assessed the effects of warmer

822   temperatures from this revised baseline. Our approach allows a simple assessment of CO_2 effects

823   exploring a range of different effect strengths. Real-world responses will likely be more complex,

824   with, for example, nutrient limitation potentially affecting the extent to which growth is stimulated by
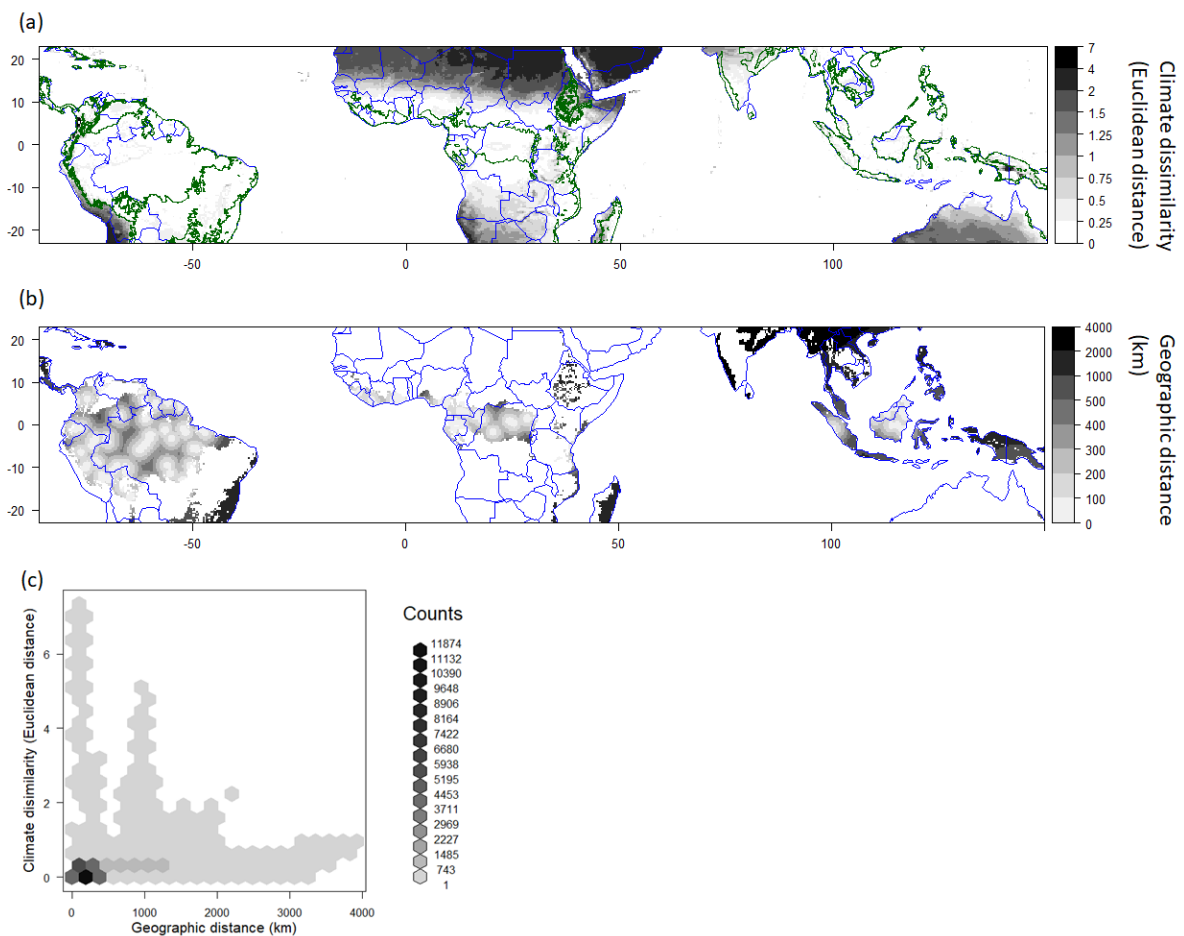
825   CO_2 (*77*).

826

827

828

17
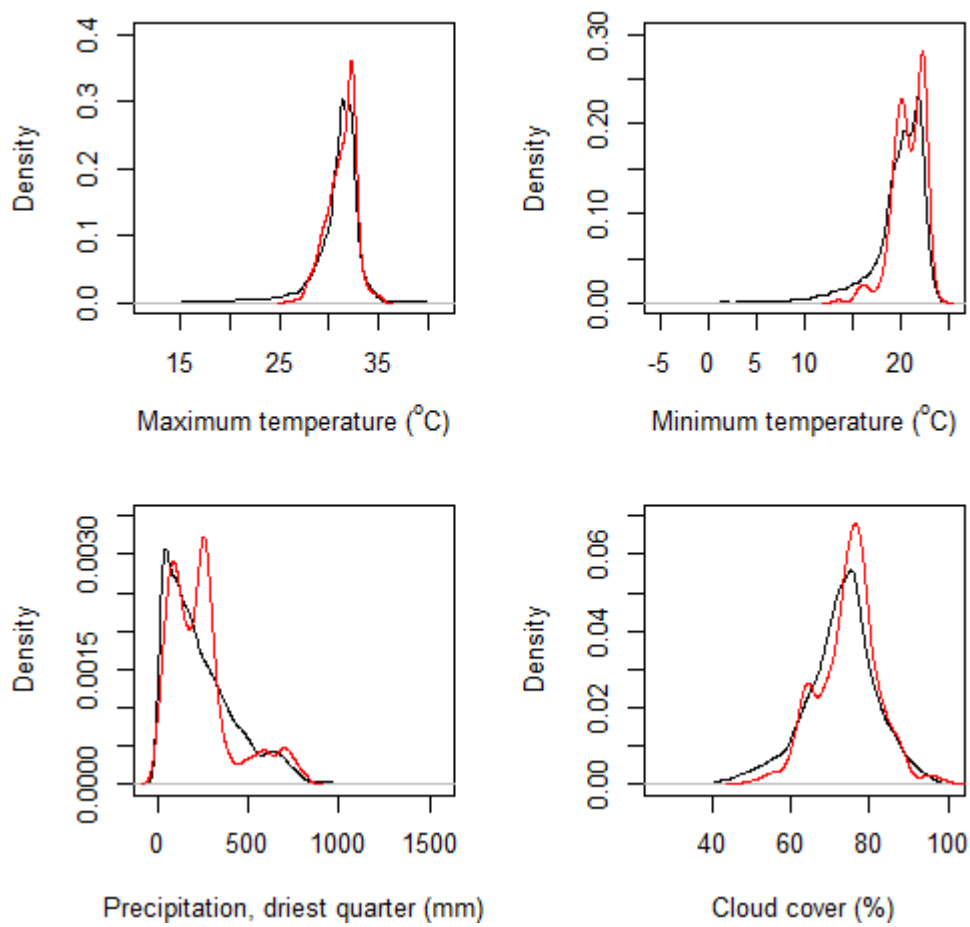
Figure S1. Climate space represented by our plot network. Red lines show the probability density function of each variable in our multi-census plot network. Black lines show the probability density across 10 minute grid-cells in the biome, restricted to areas with forest cover in GLC 2000 (*78*).

18

834

835

Figure S2. Ability of our plot network to represent the climate conditions found in the moist tropical forest biome. (a) Minimum climate dissimilarity (measured as Euclidean distance on climate variables scaled by their standard deviation) between 10 minute grid cells and the multi-census plot network. Climate variables used are the same as in Fig. 2. Green lines indicate the extent of the biome. (b) Geographic distance (km) between grid cells and the multi-census plot network. (c) Relationship between climatic and geographic distance of 10 minute grid cells across the tropical forest biome to our plot network. The lack of relationship between climate dissimilarity and geographical distance, alongside the mostly low climatic dissimilarities, shows that our sampling is sufficient to capture the environmental space of the biome and that we can reasonably extrapolate to geographically distant areas from our plots, which are in any case largely deforested already and hence contribute very little to our projected biome-wide carbon response to climate change. (These tropical moist forest areas that are poorly sampled and largely lost include the Atlantic Forests in Brazil, Andean Forests in western

19

848   South America, eastern Caribbean, Madagascar, and much of tropical South Asia, south China,

849   continental Southeast Asia, Philippines, Sumatra and Java).

850
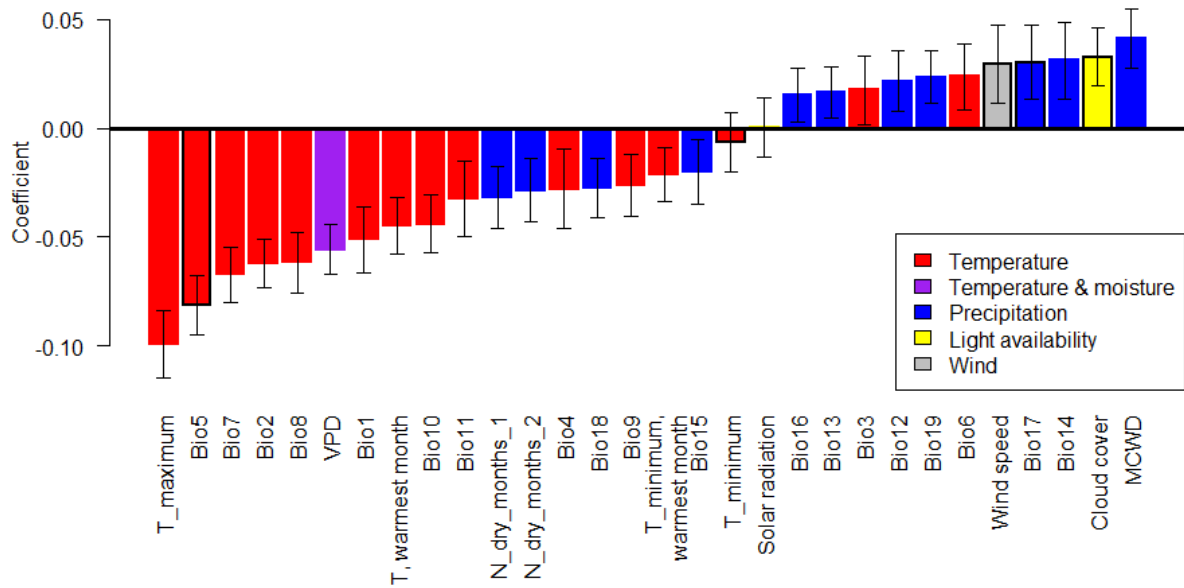
851

852 **Figure S3.** Relationships between individual climate variables and tropical forest aboveground carbon

853 stocks. Standardised coefficients are from models with the climate variable and continent as

854 explanatory variables and show change in ln(carbon) for a standard deviation change in the

855 explanatory variable. Error bars show standard errors. Variables used in the main analysis have black

856 outlines. Full variable names are: T_maximum – mean daily maximum temperature, Bio5 – mean

857 daily maximum temperature in the warmest month, Bio7 – annual temperature range, Bio2 – mean

858 diurnal temperature range, Bio8 – mean temperature in the wettest quarter, VPD – vapour pressure

859 deficit, Bio1 – mean annual temperature, Bio10 – mean temperature in the warmest quarter, Bio11 –

860 mean temperature in the coldest quarter, N_dry_months_1 – number of months with negative

861 cumulative water deficit, N_dry_months_2 – number of months where precipitation is less than

862 evapotranspiration, Bio4 – temperature seasonality, Bio18 – precipitation in the warmest quarter, Bio9

863 – mean temperature in the driest quarter, T_minimum warmest month – mean daily minimum

864 temperature in the warmest month, Bio15 – precipitation seasonality, T_minimum – mean daily

865 minimum temperature, Bio16 – precipitation in the wettest quarter, Bio13 – precipitation in the

866 wettest month, Bio3 – isothermality, Bio12 – annual precipitation, Bio19 – precipitation in the coldest

867 quarter, Bio6 – mean daily minimum temperature in the coldest month, Wind speed – mean daily

868   wind speed, Bio17 – precipitation in the driest quarter, Bio14 – precipitation in the driest month,

869   Cloud cover – proportion of MODIS passes with cloud present, MCWD – maximum cumulative

870   water deficit (note this is negative when water deficit is high, so a positive relationship with MCWD

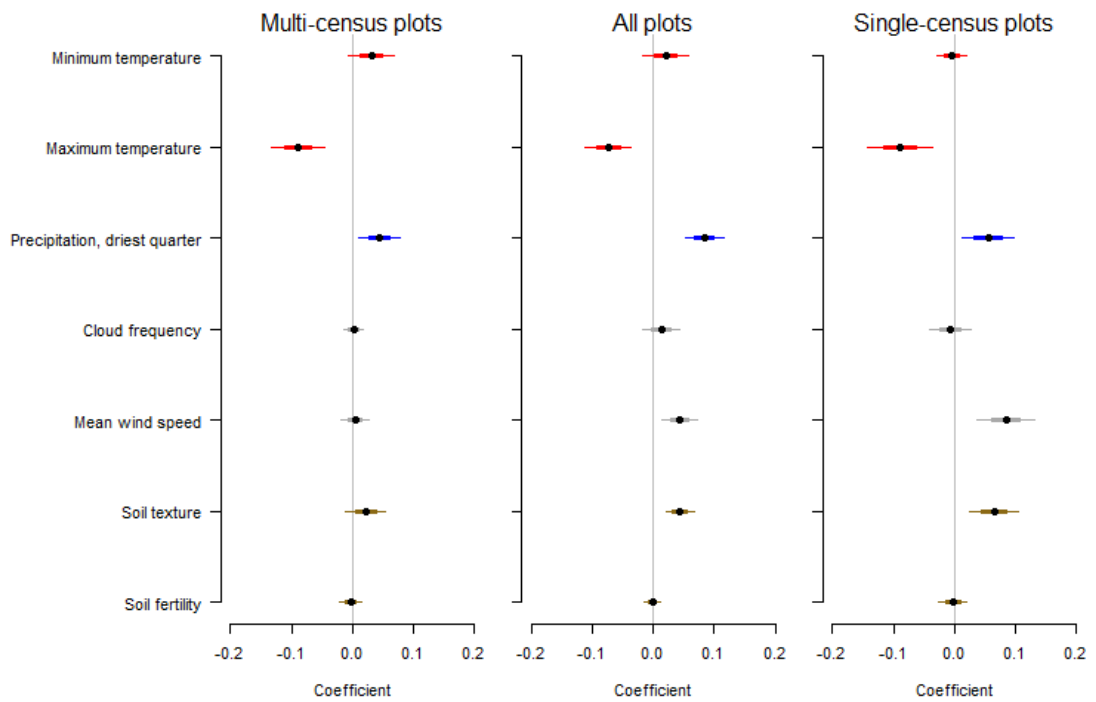871   indicates higher carbon when water deficits are less).

872

873

874

875

876

Figure S4. Validation of tropical forest carbon stock sensitivity model against an independent dataset

of 223 single-census plots from our networks measured with the same protocols. Model-averaged

shrinkage adjusted coefficients from multiple regression models of biomass carbon stocks as a

function of climate, soil, biogeography and spatial eigenvectors. Models were either fitted to the

multi-census plot dataset (as in Fig. 2), to the single-census plot dataset, or to the combined dataset.

This analysis shows that the relationships identified to be most important in the main multi-census

plot analysis (i.e. the negative relationship between carbon stocks and maximum temperature and

positive relationship with precipitation in the driest quarter) are also found in an independent dataset,

which was not used for preliminary analysis so did not influence the choice of explanatory variables.

886

3
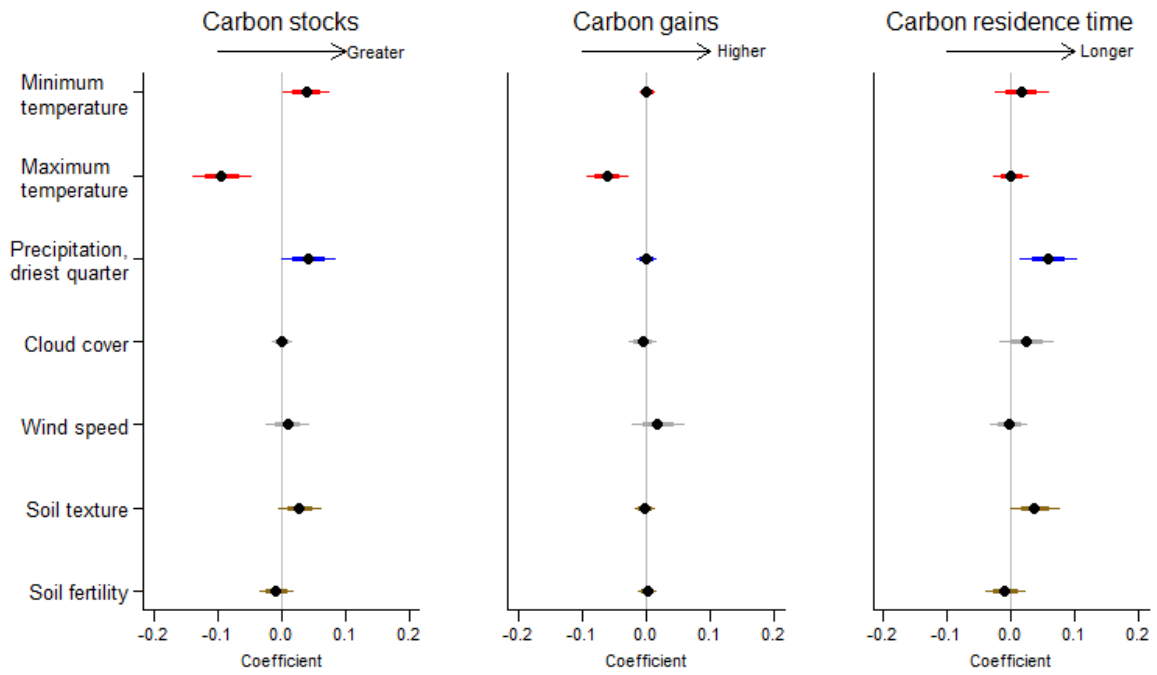
Figure S5. As Figure 2, but with aboveground biomass estimated using the Chave et al. 2005 (*79*) moist forest allometric equation, which does not include a height term and is instead based on a third-order polynomial relationship between diameter and aboveground biomass. This indicates that our results are robust to using an alternative allometry to estimate aboveground biomass.

893

894
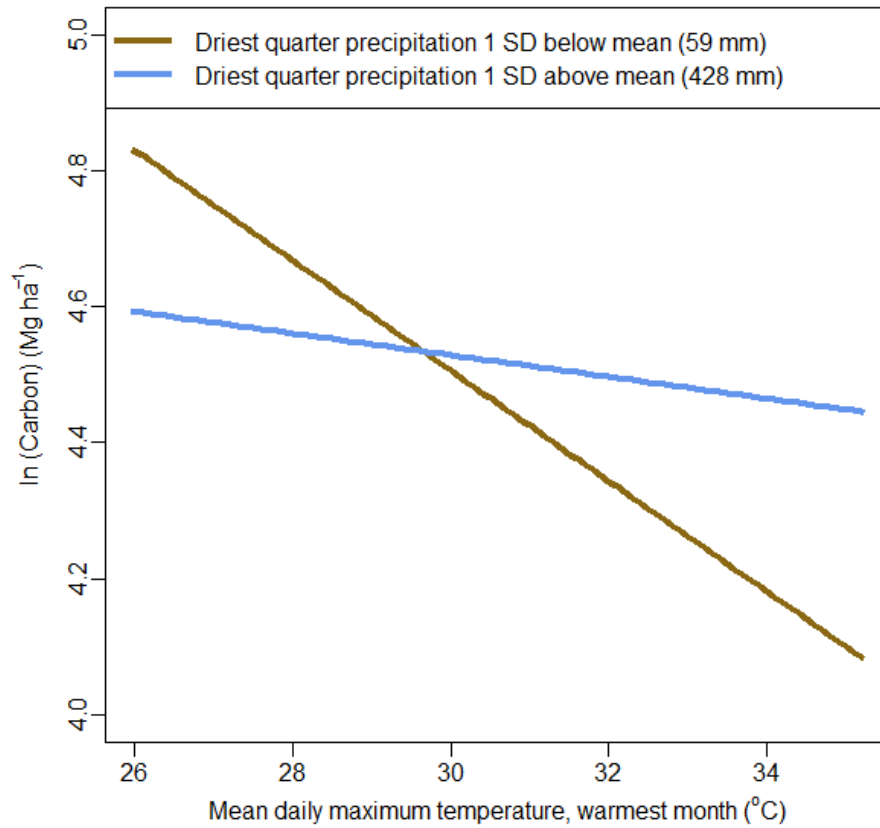
895

896 **Figure S6.** Interaction between mean daily maximum temperature in the warmest month and

897 precipitation in the driest quarter in determining aboveground tropical forest carbon stocks. Modelled

898 relationships with temperature are shown holding precipitation either one standard deviation above or

899 below the mean. Note that the temperature-carbon relationship is steeper when precipitation is low.

900

901
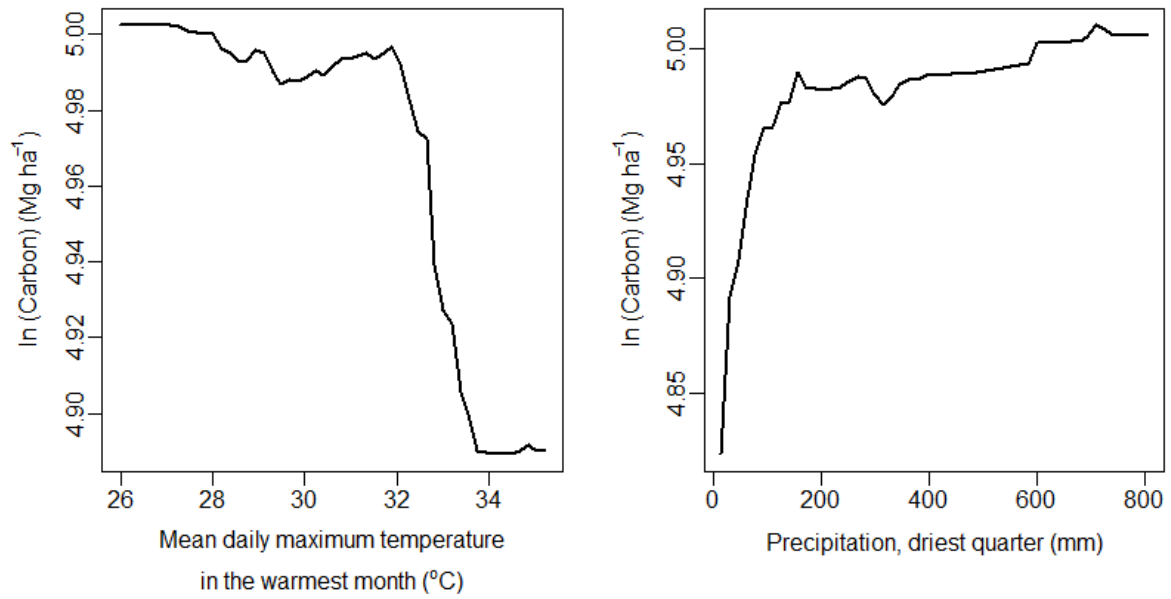
902

903 **Figure S7.** Partial relationships between tropical forest carbon stocks and the two climate variables

904 identified to be most important by the random forest decision tree algorithm. Partial plots show

905 predicted values of carbon stocks averaged across an ensemble of decision tree models when

906 changing the explanatory variable of interest and holding other variables constant. The importance of

907 variables in random forest analysis is assessed by calculating the average increase in node purity

908 across all decision trees (measured by residual sum of squares) when using the variable to split the

909 data. Higher values indicate greater importance. Maximum temperature increased node purity by 4.8

910 and precipitation by 4.7. For all other climate variables increases in node purity were < 3.5.

911
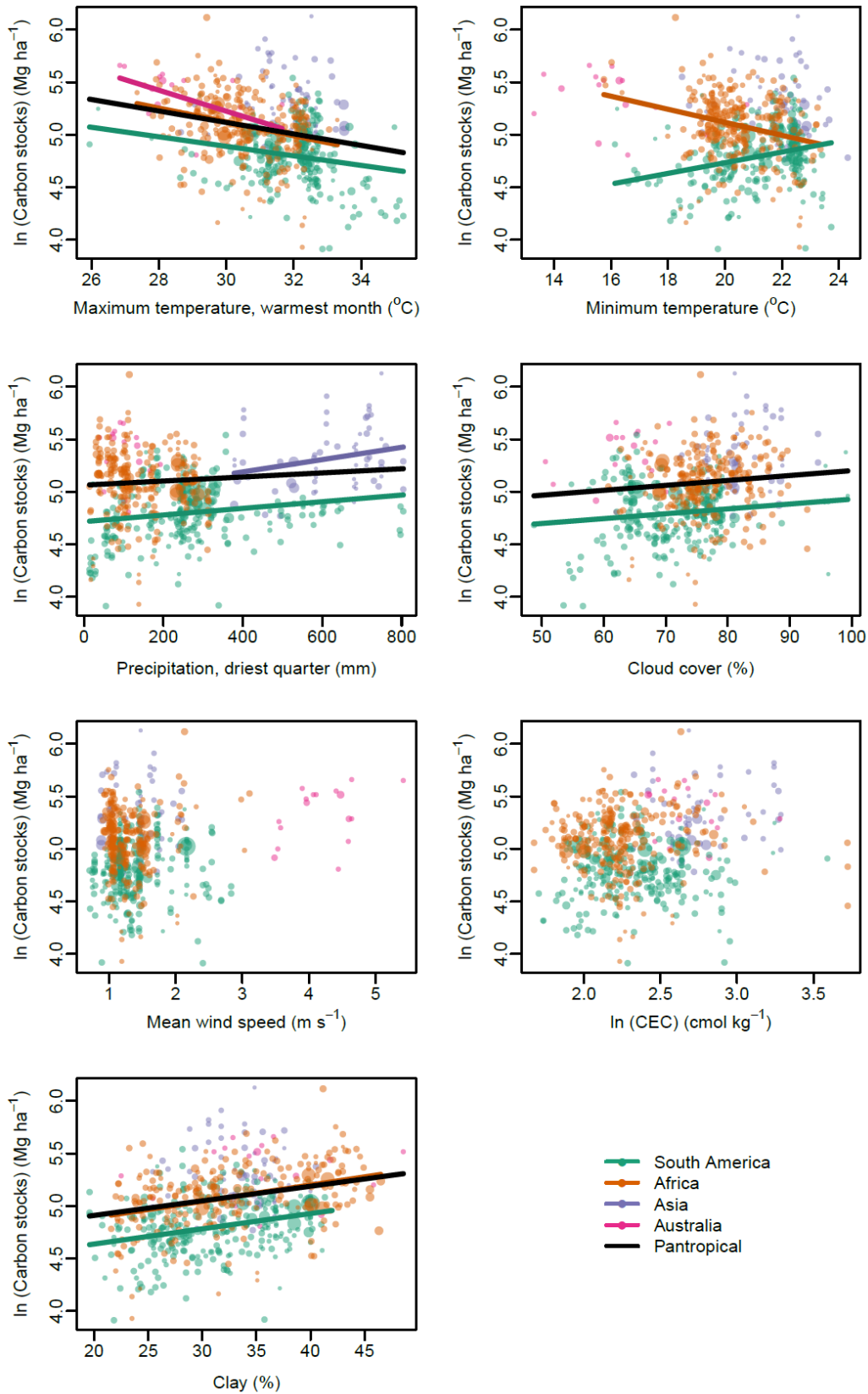
**Figure S8.** Relationships between aboveground tropical forest carbon stocks and environmental

predictors. Symbols and colours as in Fig. 3. Coloured lines show bivariate relationships in each

7

915   continent, and black lines show pan-tropical relationships also accounting for the effect of continent.

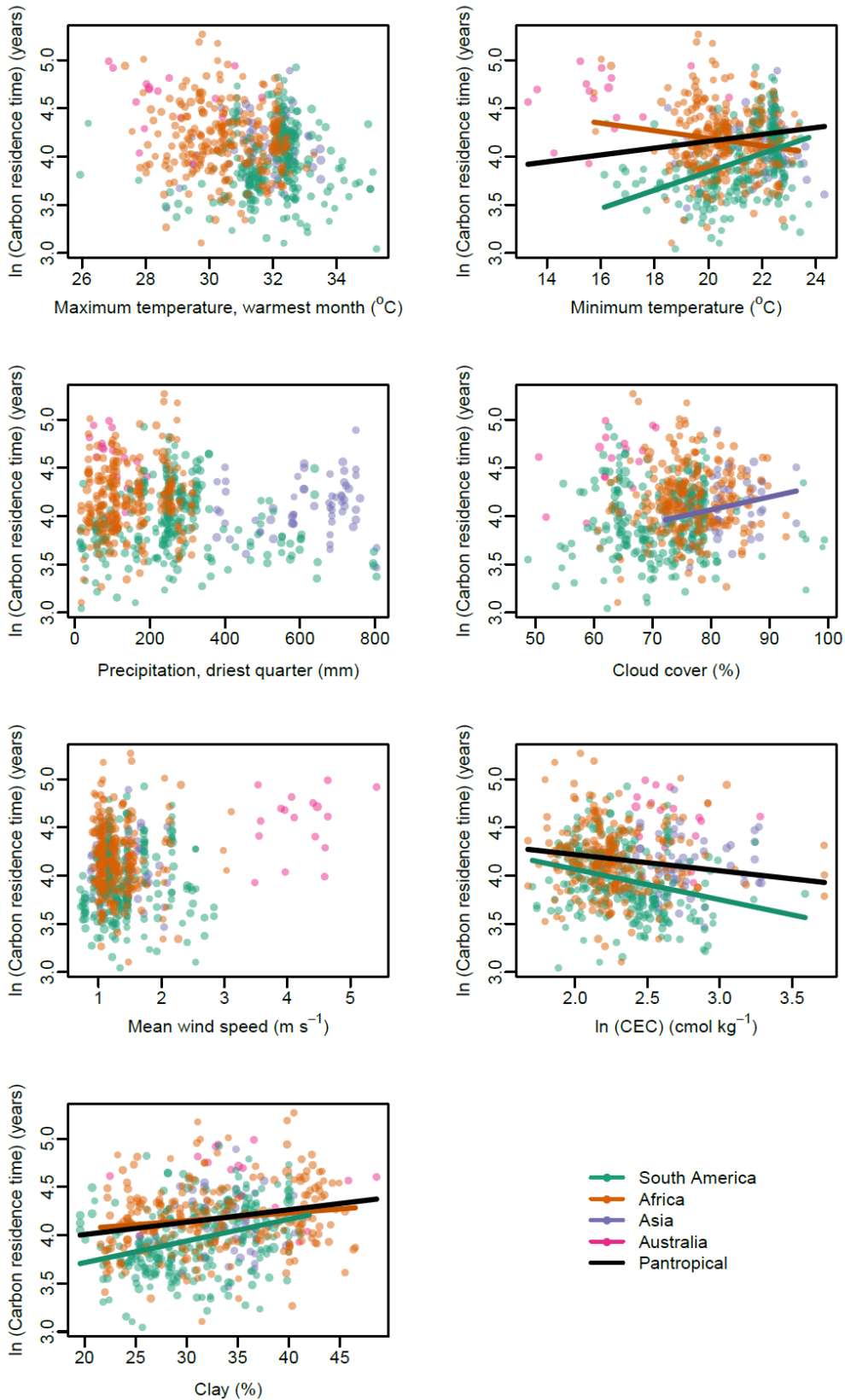916   Lines are only plotted where statistically significant.

917
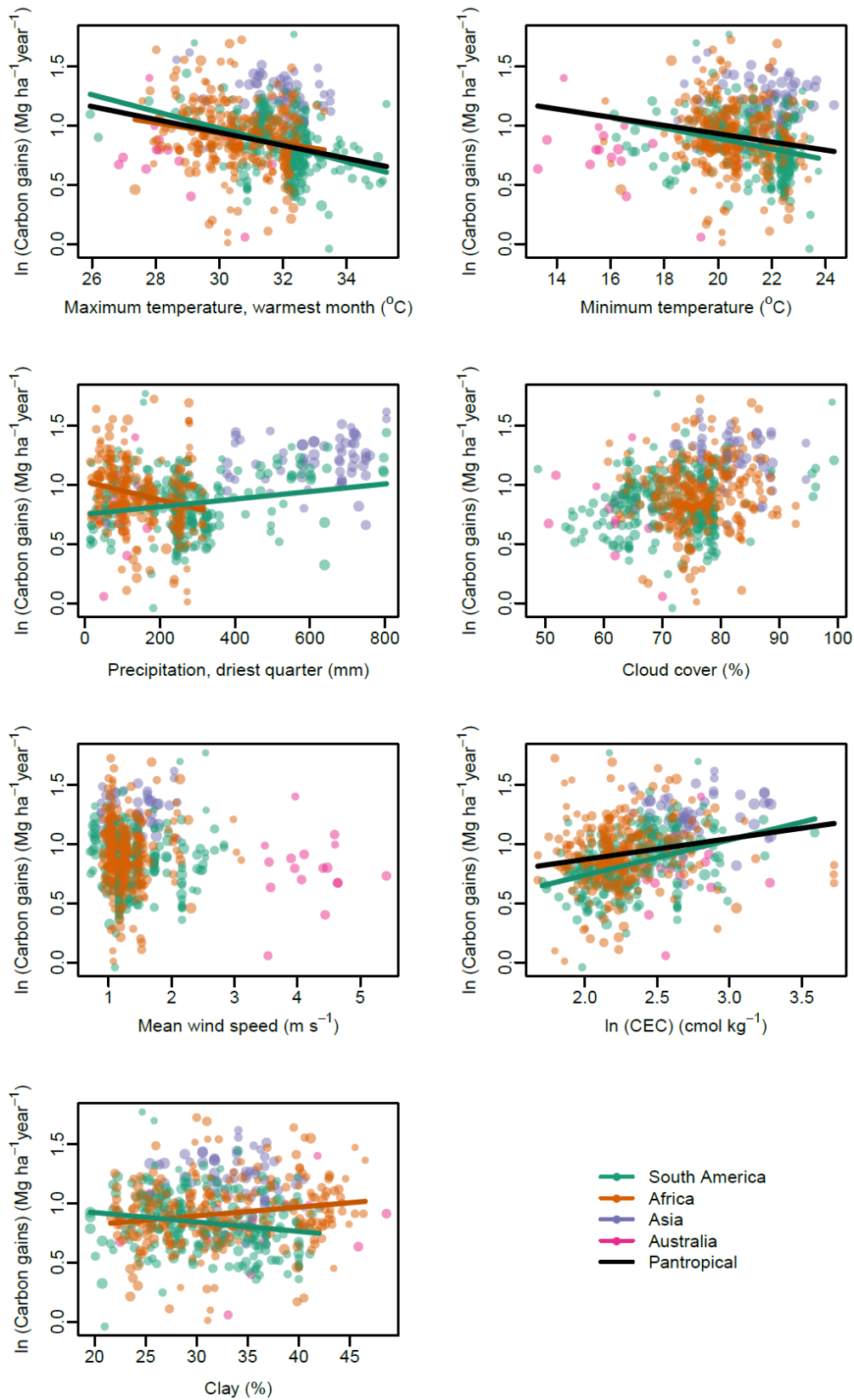
918
919
920 **Figure S9.** As Fig. S8, but showing relationships with carbon gains.

Figure S10. As Fig. S8, but showing relationships with carbon residence time.
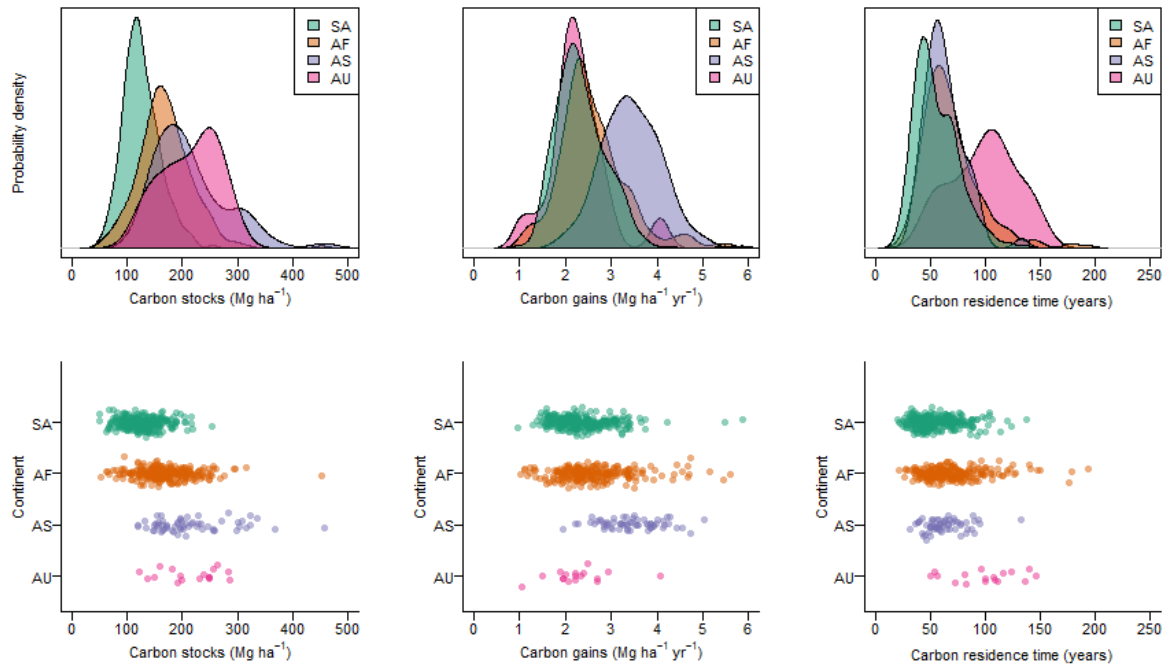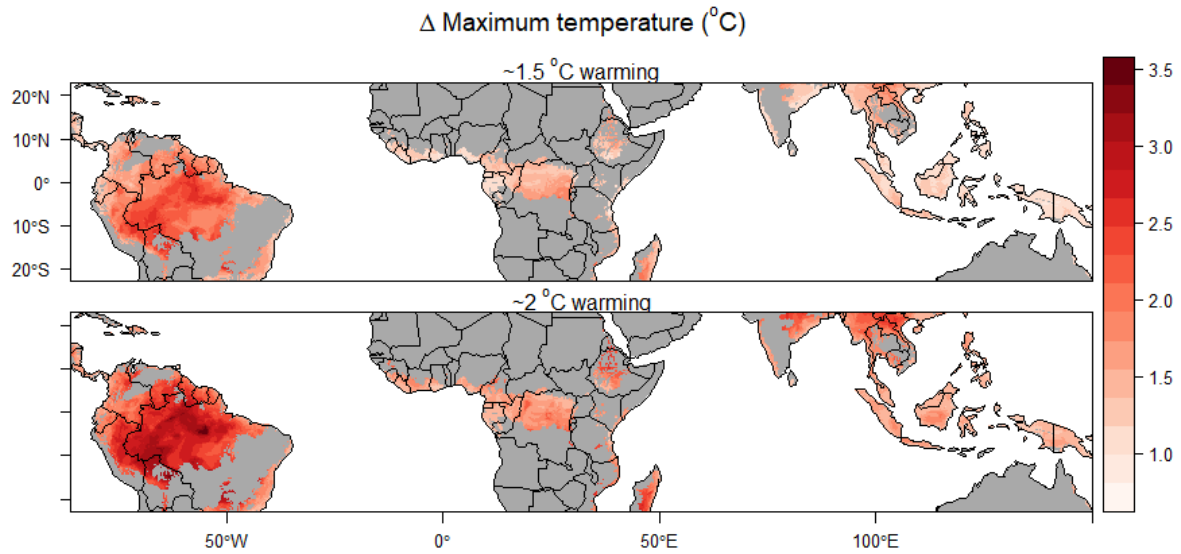
Figure S11. Variation in tropical forest aboveground carbon stocks, gains and residence time within and amongst continents. Data are presented as empirical probability density functions (top row) and dot-plots showing raw data points for all our multi-census plots (bottom row). SA = South America, AF = Africa, AS = Asia, AU = Australia.

Figure S12. Biome-wide change in mean daily maximum temperature in the warmest month from present conditions (based on the Worldclim climatology, 1970-2000), given global increases in temperature of approximately 1.5°C and 2°C above pre-industrial levels. These levels of global temperature increase are obtained from, respectively, RCP 2.6, 2040-2060 and RCP 4.5, 2040-2060. Global temperature increases of 1.5 and 2°C above pre-industrial levels (so ~0.8 °C and ~1.3 °C above our current baseline climate) would lead to mean increases in maximum temperature in the warmest month across the tropical forest biome of 1.9°C and 2.4°C the current baseline climate respectively.

941
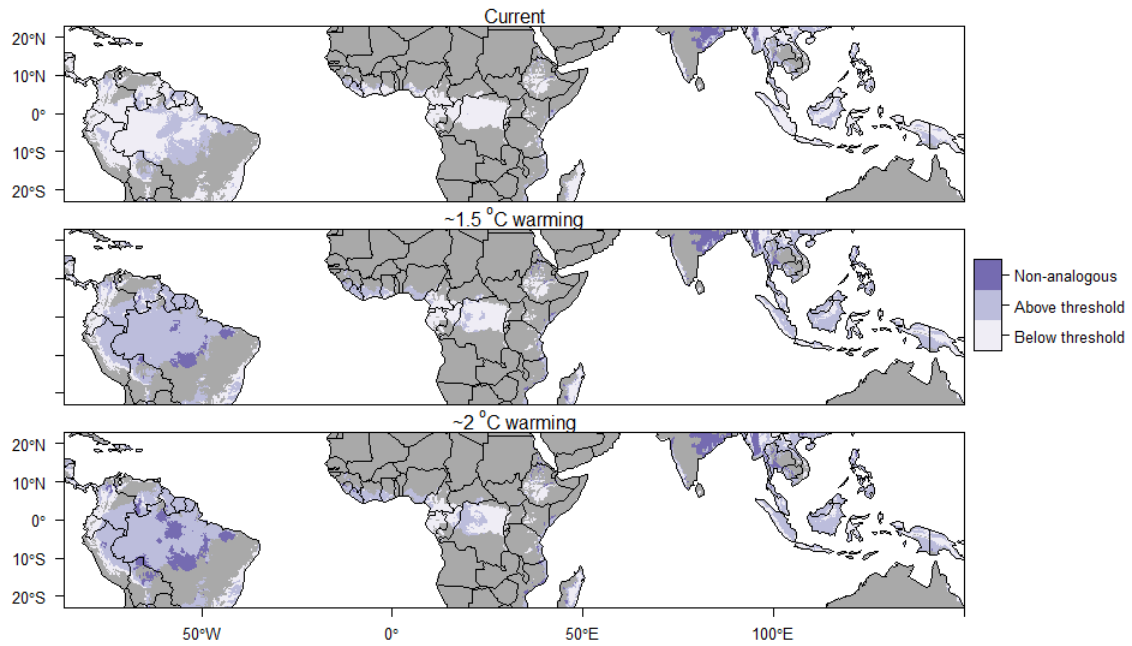
942

943 **Figure S13** Areas of the biome above or below the 32.2°C threshold, above which carbon stocks

944 decline more rapidly with temperature, under current conditions and two warming scenarios (see Fig.

945 4). Areas warmer than any currently observed in our dataset (35.2°C) are also shown (non-analogous

946 conditions). Note that even the 1.5°C warming scenario pushes most South American forests above

947 the 32.2°C threshold.

948
949
950
951
952
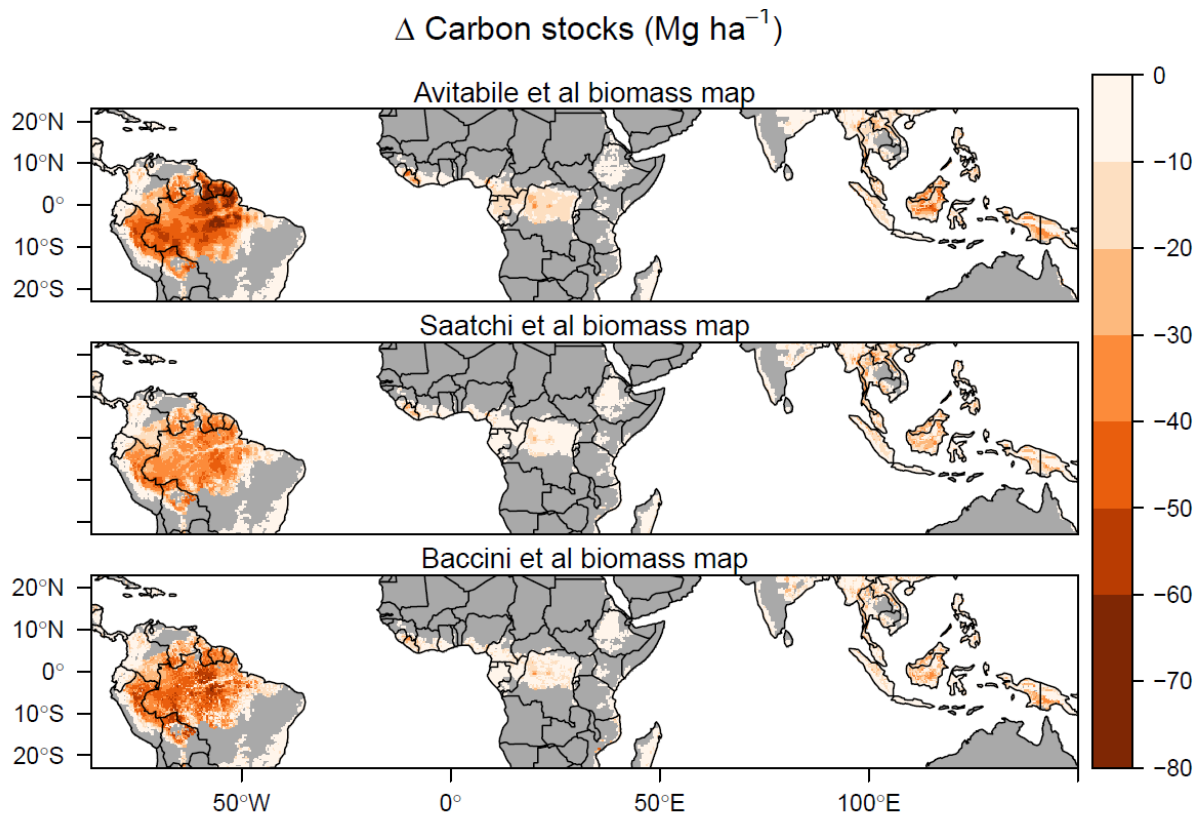
Figure S14. Effect of using earlier biomass reference maps for estimates of change in long-term carbon stocks for global temperature increases of ~2°C. Using aboveground biomass stock maps from Saatchi et al. (*65*) and Baccini et al. (*66*) predicted biome-wide reductions in biomass carbon stocks are 24.0 Pg (95 % CI = 5.8 – 39.6) and 28.4 Pg (95 % CI = 16.1 – 37.5) respectively. Under the ~ 1.5°C warming scenario these are 18.4 Pg (5.8 – 30.5) and 21.1 Pg (10.2 – 29.4) respectively. Results in the main text use the 2016 Avitabile et al. baseline map (*30*) – see methods for justification.
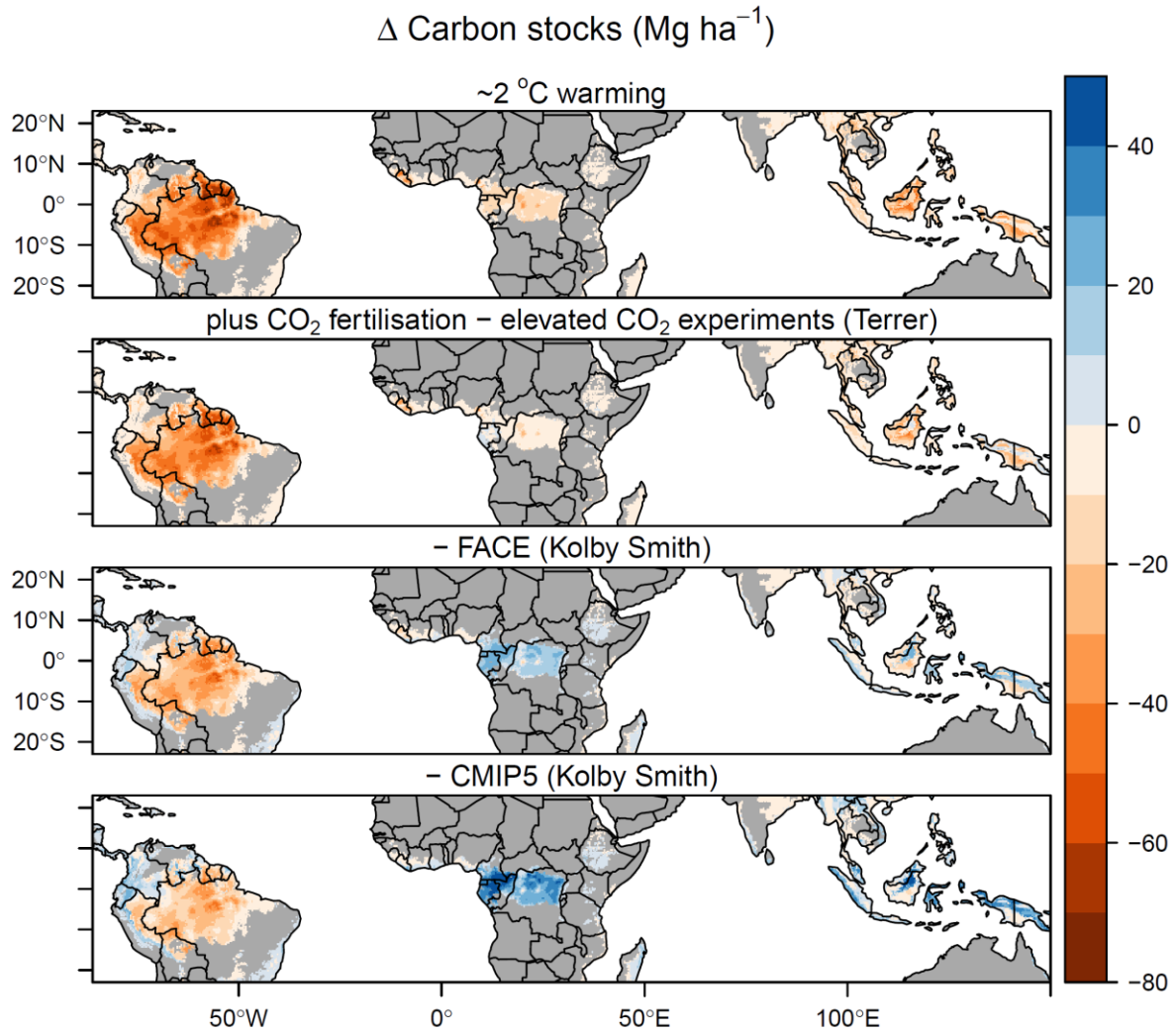
Figure S15. Predicted long-term change in aboveground carbon stocks under $\sim 2°C$ global warming, based on either temperature effects alone or when also accounting for carbon dioxide growth stimulation. CO_2 fertilisation effects on equilibrium biomass levels were obtained from a recent synthesis of results of elevated CO_2 experiments (Terrer et al. (*77*)), free-air CO_2 enrichment (FACE) experiments (Kolby Smith et al. (*74*)) and CMIP5 earth system models (Kolby Smith et al. (*74*)). Depending on their strength, CO_2 effects either partially or fully ameliorate the biome-wide negative effects of increasing temperatures on biomass carbon stocks (Table S3), but these carbon stocks are predicted to decline over much of Amazonia even under the strongest CO_2 effect considered.

15

972 **Table S1.** Climate variables selected for analysis and mechanisms by which they can affect carbon stocks.

Climate property	Variable selected for analysis	Mechanism to affect carbon stocks
Daytime temperature	Maximum temperature in the warmest month[1]	High daytime temperatures exceed photosynthesis optima (*80*), increase evaporative stress, causing stomatal closure and reducing time for photosynthesis (*26*) and increase risk of mortality through hydraulic failure and/or carbon starvation (*23*).
Night-time temperature	Mean daily minimum temperature	Respiration rate increases with temperature so proportion of carbon taken through photosynthesis that is allocated to wood should decline with temperature (*81*). Increased respiration cost could also reduce tree longevity (*23*). As respiration occurs day and night, and photosynthesis only in the day, nighttime temperature should better reflect respiration effects and daytime temperature better reflect photosynthesis effects.
Moisture availability	Precipitation in the driest quarter[2]	Moisture availability could limit photosynthesis and hence carbon gains, with stomata closing when moisture availability is limiting. The risk of mortality through hydraulic failure or carbon starvation is higher when moisture is limiting (*23*), and this could also set a limit on potential tree size and hence tree longevity.
Light availability	Cloud frequency	Increased photosynthesis and hence AGWP when light availability is greatest (i.e. cloud cover is low) (*82*). Alternatively, light availability could have a negative effect due to high evapotranspiration stress when cloud cover is low.
Wind speed	Mean wind speed	Carbon stocks are expected to be lower where physical damage through wind throw or breakage is higher, as carbon is removed more quickly from the system through mortality (*83*). But there is potential for greater carbon gains if forests are more dynamic.

973 [1] Mean daily temperature in the warmest month (bio5) was selected instead of mean daily maximum temperature as it was more strongly decoupled from
974 other climate variables. VPD could also represent some of these effects, but was too strongly correlation with maximum temperature to include as an
975 independent variable.

976 [2] Moisture availability could also be represented by MCWD (maximum cumulative water deficit) or total precipitation, but only one of the three variables
977 could be included in the model due to collinearity. MCWD was excluded as it is zero truncated, so less amenable to regression fitting.

978

979 **Table S2.** Coefficients of model-averaged general linear models of carbon stocks, gains and residence time as a function of climate, soil, continent and spatial
980 autocorrelation. Coefficients are AIC weighted averages across models with $\Delta AIC < 4$ from the best performing model; variables are given a score of zero if
981 they did not appear in a model. NA indicates that a term did not occur in any model in this set. MEM1-8 are spatial eigenvectors.

	Carbon stocks				Carbon gains				Carbon residence time			
Variable	Estimate	SE	Z	P	Estimate	SE	Z	P	Estimate	SE	Z	P
Intercept - Africa	4.986	0.010	476.9	<0.001	0.571	0.525	1.09	0.278	3.909	0.688	5.67	<0.001
Minimum temperature	0.031	0.019	1.67	0.096	-0.001	0.007	0.18	0.861	0.019	0.022	0.88	0.381
Maximum temperature, warmest month	-0.089	0.022	4.11	<0.001	-0.060	0.017	3.47	<0.001	-0.001	0.015	0.10	0.924
Precipitation, driest quarter	0.045	0.018	2.54	0.011	-0.001	0.008	0.14	0.887	0.061	0.023	2.70	0.007
Cloud frequency	0.002	0.008	0.24	0.814	-0.006	0.011	0.54	0.592	0.025	0.021	1.17	0.241
Wind speed	0.004	0.012	0.38	0.705	0.016	0.020	0.78	0.437	-0.004	0.015	0.24	0.807
Soil texture (% clay)	0.021	0.017	1.26	0.208	-0.005	0.011	0.49	0.628	0.040	0.018	2.17	0.030
Soil fertility (CEC)	-0.003	0.009	0.34	0.732	0.005	0.011	0.51	0.613	-0.012	0.017	0.70	0.486
MEM1	0.115	0.014	7.96	<0.001	0.319	0.559	0.57	0.569	0.375	0.734	0.51	0.610
MEM2	0.098	0.017	5.67	<0.001	0.083	0.273	0.30	0.762	0.286	0.359	0.80	0.427
MEM3	-0.025	0.014	1.84	0.065	0.014	0.041	0.34	0.735	0.007	0.054	0.12	0.904
MEM4	-0.021	0.011	1.84	0.066	-0.038	0.020	1.84	0.066	-0.002	0.027	0.07	0.945
MEM5	0.027	0.011	2.46	0.014	0.020	0.015	1.33	0.182	0.020	0.020	0.98	0.327
MEM6	0.017	0.011	1.56	0.118	0.025	0.011	2.34	0.019	-0.014	0.014	1.05	0.293
MEM7	0.010	0.011	0.93	0.353	-0.017	0.010	1.61	0.107	0.036	0.014	2.57	0.010
MEM8	-0.072	0.013	5.64	<0.001	0.057	0.012	4.91	<0.001	-0.127	0.016	7.80	0.000
Asia	NA				0.380	0.542	0.70	0.485	-0.753	0.683	1.10	0.271
Australia	NA				-0.173	0.390	0.44	0.658	0.006	0.516	0.01	0.990
South America	NA				0.643	1.164	0.55	0.582	0.542	1.530	0.35	0.724

982

2

983 **Table S3.** Predicted biome-wide changes in long-term biomass carbon stocks (scaled to include root

984 biomass) under global temperature increases of ~ 1.5°C and ~ 2°C. Changes are based on temperature

985 effects alone, and when also accounting for the effect of increased CO_2 concentrations on tree growth.

986 CO_2 effects were obtained from a synthesis of results of elevated CO_2 experiments (Terrer et al. (*77*)),

987 free-air CO_2 enrichment (FACE) experiments (Kolby Smith et al. (*74*)) and CMIP5 earth system

988 models (Kolby Smith et al. (*74*)). 95% confidence intervals around changes (based on uncertainties in

989 temperature effects alone) are shown in parentheses.

CO_2 effect	Change in biomass carbon stocks (Pg)	
	~ 1.5°C warming (443 ppm CO_2)	~ 2°C warming (487 ppm CO_2)
None	-26.9 (-38.4 - -15.8)	-35.3 (-49.0 - -20.9)
Terrer et al. elevated CO_2 experiments	-22.0 (-33.0 - -9.9)	-26.3 (-37.6 - -11.5)
Kolby Smith et al. FACE experiments	-6.2 (-16.8 – 7.7)	-9.9 (-24.3 – 3.9)
Kolby Smith et al. CMIP5 models	3.9 (-8.3 – 12.6)	2.0 (-11.9 – 19.8)

990

991

992

993

4